universe

MDPI

Review

Probing the Interior of the Schwarzschild Black Hole Using Congruences: LQG vs. GUP

Saeed Rastgoo [1,*] and Saurya Das [2]

[1] Department of Physics and Astronomy, York University, 4700 Keele Street, Toronto, ON M3J 1P3, Canada
[2] Theoretical Physics Group and Quantum Alberta, Department of Physics and Astronomy, University of Lethbridge, 4401 University Drive, Lethhbridge, AB T1K 3M4, Canada; saurya.das@uleth.ca
* Correspondence: srastgoo@yorku.ca

Abstract: We review, as well as provide some new results regarding the study of the structure of spacetime and the singularity in the interior of the Schwarzschild black hole in both loop quantum gravity and generalized uncertainty principle approaches, using congruences and their associated expansion scalar and the Raychaudhuri equation. We reaffirm previous results that in loop quantum gravity, in all three major schemes of polymer quantization, the expansion scalar, Raychaudhuri equation and the Kretschmann scalar remain finite everywhere in the interior. In the context of the eneralized uncertainty principle, we show that only two of the four models we study lead to similar results. These two models have the property that their algebra is modified by configuration variables rather than the momenta.

Keywords: quantum gravity; quantum black hole; loop quantum gravity; generalized uncertainty principle; singularity resolution; Raychaudhuri equation

Citation: Rastgoo, S.; Das, S. Probing the Interior of the Schwarzschild Black Hole Using Congruences: LQG vs. GUP. *Universe* **2022**, *8*, 349. https://doi.org/10.3390/universe8070349

Academic Editor: Włodzimierz Piechocki

Received: 8 May 2022
Accepted: 22 June 2022
Published: 24 June 2022

1. Introduction

Black holes are one the most important objects in the Universe with regards to quantum gravity. The singularity in their interior is a prediction of general relativity (GR), which in turn is a prediction of its eventual breakdown. Furthermore, it is believed that this singularity resides in a small spatial region where quantum effects cannot be neglected. Thus, one has the natural expectation that a final theory of quantum gravity should be able to resolve this singularity. Various theories of quantum gravity or effective gravity have been utilized to study such objects. Among these are loop quantum gravity (LQG) [1], a nonperturbative canonical theory of quantization of the gravitational field, and the generalized uncertainty principle (GUP), which is a rather phenomenological approach resulting from the assumption of noncommutativity of spacetime or existence of a minimum length.

In LQG, there have been numerous works studying both the interior and the full spacetime of the Schwarzschild black hole [2–41]. In particular, the interior of such a black hole has been studied in various ways. One of the most common approaches uses the so called polymer quantization [42–46], which was originally inspired by loop quantum cosmology (LQC), dealing with a certain quantization of the isotropic Friedmann-Lemaitre-Robertson-Walker (FLRW) model [47,48]. Since the interior of the Schwarzschild black hole is isometric to the Kantowski-Sachs cosmological model, the idea in this polymer approach is to apply the same techniques of the polymer quantization of the Kantowski-Sachs model to the Schwarzschild interior [49,50]. Polymer quantization introduces a parameter in the theory called the polymer scale, that sets the minimal scale of the model close to which the quantum gravity effects become important. The approach in which such a parameter is taken to be constant is called the μ_0 scheme (which in this paper we refer to as the $\mathring{\mu}$ scheme), while approaches where it depends on the phase space variables are denoted by $\bar{\mu}$ schemes. The various approaches were introduced to deal with some important issues resulting from quantization, namely, to have the correct classical limit (particularly in LQC),

to avoid large quantum corrections near the horizon, and to have final physical results that are independent of auxiliary or fiducial parameters. Other approaches to this model in LQG such as Refs. [51,52] provide a derivation of a Schwarzschild black hole modified dynamics, not relying on minisuperspace models. Starting from the full LQG theory, this model performs the symmetry reduction at the quantum level. This has led to several differences in the effective dynamics with respect to previous polymer quantization-inspired models, one of which is the absence of the formation of a white hole in the extended spacetime region replacing the classical singularity. All of these past studies in LQG and some other approaches point to the resolution of the singularity at the effective level.

Another approach to quantum gravity uses the so-called Generalized Uncertainty Principle (GUP). GUP extends the standard canonical commutation relation to include additional (small) momentum dependent terms, such that Heisenberg's uncertainty principle gets modified as well. It can be shown that as a result, there must exist a minimum measurable length, which can be for example, a multiple of the Planck length. Furthermore, such a modification affects practically all quantum Hamiltonians, even at low energies, giving rise to potentially measurable predictions of various quantum gravity theories [53–58]. It may be noted that in the infrared limit, there is also an Extended Uncertainty Principle (EUP) which may apply to the black hole spacetimes under consideration [59–65].

A particularly powerful approach to study the singularities in classical and semiclassical/effective gravity is the use of congruences and the associated expansion scalar and the Raychaudhuri equation to probe the structure of spacetime. This approach which is the backbone of the Hawking–Penrose singularity theorem, was particularly used, among other works, in several of our recent studies [36,55,66]. In this approach, a particular choice of congruence is made by choosing the velocity vector field of the associated geodesics. In previous works we have mainly used timelike congruences, while here we systematically use both timelike and null ones.

This paper serves as both a review of our recent works in studying the congruences in the interior of the Schwarzschild black hole in LQG and GUP approaches, and also includes new results, particularly with regard to GUP and the nonperturbative behavior of the Kretschmann scalar in both approaches. The structure of the paper is as follows: In Appendix A, we brief review the geodesic deviation, expansion scalar and the Raychaudhuri equation and their significance in studying the structure of spacetime. In Section 2 we use these results to choose certain congruences to study the interior of the Kantowski-Sachs metric which is isometric to the Schwarzschild black hole interior. In Section 3 we review the classical formulation of the interior of the Schwarzschild balck hole based on the Ashtekar-Barbero connection and derive general expressions for the expansion scalar and the Raychaudhuri equation for both timelike and null cases. In Section 4.1 we apply these results to the effective black hole interior in LQG and show that in all the three common schemes, and using either timelike or null congruences, not only expansion scalar and the Raychaudhuri equation always remain finite in the interior, but also the Kretschmann scalar does so. In Section 4.2, we do the same for four most common model in GUP and show that only two of them have the property that their expansion scalar and Raychaudhuri equation together with he Kretschmann scalar always remain finite. Finally, in Section 5, we conclude and present an outlook for future work.

2. General Schwarzschild Interior and Congruences

Given that the radial spacelike and timelike coordinates switch their causal nature one we cross the horizon in the Schwarzschild black hole, we can simply switch $t \leftrightarrow r$ in the Schwarzschild metric to obtain the metric of the interior as

$$ds^2 = -\left(\frac{2GM}{t} - 1\right)^{-1} dt^2 + \left(\frac{2GM}{t} - 1\right) dr^2 + t^2 d\Omega^2, \tag{1}$$

where t, r, θ, ϕ are the standard Schwarzschild coordinates and $d\Omega^2 = d\theta^2 + \sin^2(\theta) d\phi^2$. As it is seen, t^2 now plays the role of the radius of the infalling 2-spheres. Notice that

this model is not a field theory anymore since the metric components (and hence the degrees of freedom) are independent of r. So we are dealing with a system with finite degrees of freedom, i.e., a minisuperspace model. The above metric is a special case of the Kantowski-Sachs cosmological model

$$ds^2_{KS} = -N(t)^2dt^2 + g_{xx}(t)dx^2 + g_{\theta\theta}(t)d\theta^2 + g_{\phi\phi}(t)d\phi^2, \tag{2}$$

which describes a homogeneous but anisotropic spacetime.

In order to obtain a general result for such models, we consider a metric of the form

$$ds^2 = -N(t)^2dt^2 + X^2(t)dr^2 + Y^2(t)d\Omega^2. \tag{3}$$

We will study the null and timelike congruences propagating on this spacetime. To be self-contained, a brief review of the geodesic deviation, expansion scalar, and Raychaudhuri equation is given in Appendix A.

2.1. Timelike Case

Let us consider a radial timelike congruence of geodesics where their velocity vector in the coordinates given in Equation (3) is

$$U^\mu = \left(U^0, U^1, 0, 0\right). \tag{4}$$

Given that U^a is a unit timelike vector field, the above vector can be written as

$$U^\mu = \left(U^0, \frac{\sqrt{-1 + N^2(U^0)^2}}{X}, 0, 0\right). \tag{5}$$

Hence, to simplify our analysis we choose the free component U^0 as

$$U^0 = \frac{1}{N}, \tag{6}$$

to obtain

$$U^\mu = \left(\frac{1}{N}, 0, 0, 0\right). \tag{7}$$

Using this form of the velocity vectors, we can easily obtain the transverse metric from Equation (A2) as

$$h_{\mu\nu} = \begin{pmatrix} 0 & 0 & 0 & 0 \\ 0 & X^2 & 0 & 0 \\ 0 & 0 & Y^2 & 0 \\ 0 & 0 & 0 & Y^2\sin^2(\theta) \end{pmatrix}. \tag{8}$$

The expansion tensor corresponding to Equation (7) also becomes

$$B_{\mu\nu} = \nabla_\nu U_\mu = \begin{pmatrix} 0 & 0 & 0 & 0 \\ 0 & \frac{X\dot{X}}{N} & 0 & 0 \\ 0 & 0 & \frac{Y\dot{Y}}{N} & 0 \\ 0 & 0 & 0 & \frac{Y\dot{Y}}{N}\sin^2(\theta) \end{pmatrix}. \tag{9}$$

Using this tensor, the metric and the transverse metric Equation (8), it is straightforward to obtain

$$\theta = \frac{\dot{X}}{NX} + 2\frac{\dot{Y}}{NY}, \tag{10}$$

$$\sigma^2 = \frac{2}{3N^2}\left(\frac{\dot{X}}{X} - \frac{\dot{Y}}{Y}\right)^2, \tag{11}$$

$$\omega_{ab} = 0. \tag{12}$$

It is clear from here that in order to be able to find these quantities, we need to obtain the equations of motions, i.e., the Einstein's equations. Here is where the difference between the classical and the effective cases show up. As we will see later, either the Hamiltonian or the canonical algebra of the interior is changed and this leads to modified equations of motion, which consequently results in modified expansion scalar and its rate of change.

We can now compute the Raychaudhuri Equation (A10) either by finding the Ricci tensor components and replacing them in the last term of Equation (A10), or simply by using the chain rule $\frac{d\theta}{d\tau} = \frac{d\theta}{dt}\frac{dt}{d\tau} = \frac{1}{N}\frac{d\theta}{dt}$. The result is

$$\frac{d\theta}{d\tau} = -\frac{\dot{N}}{N^3}\frac{\dot{X}}{X} + \frac{1}{N^2}\frac{\ddot{X}}{X} - \frac{1}{N^2}\left(\frac{\dot{X}}{X}\right)^2 - 2\frac{\dot{N}}{N^3}\frac{\dot{Y}}{Y} + \frac{2}{N^2}\frac{\ddot{Y}}{Y} - \frac{2}{N^2}\left(\frac{\dot{Y}}{Y}\right)^2 \tag{13}$$

2.2. Null Case

In this case we choose a congruence of radial null geodesics and due to the null property of their tangent vector k^a, we obtain

$$k^\mu = \left(k^0, -\frac{Nk^0}{X}, 0, 0\right). \tag{14}$$

A simplifying choice for k^0 is thus $k^0 = \frac{1}{N}$ which results in

$$k^\mu = \left(\frac{1}{N}, -\frac{1}{X}, 0, 0\right). \tag{15}$$

The auxiliary radial null vector field l^a has two nonvanishing components that can be fixed by using the null property of l^a and the condition Equation (A14). This way we obtain

$$l^\mu = \left(\frac{1}{2N}, \frac{1}{2X}, 0, 0\right) \tag{16}$$

Using these vectors and the spacetime metric, we can find the transverse metric Equation (A15) as

$$h_{\mu\nu} = \begin{pmatrix} 0 & 0 & 0 & 0 \\ 0 & 0 & 0 & 0 \\ 0 & 0 & Y^2 & 0 \\ 0 & 0 & 0 & Y^2\sin^2(\theta) \end{pmatrix} \tag{17}$$

which is a two dimensional metric as it should be. Next, we can compute B_{ab} as in Equation (A16) and then find $\tilde{B}_{ab}$ using B_{ab} and k^a, l^a above as

$$\tilde{B}_{\mu\nu} = \begin{pmatrix} 0 & 0 & 0 & 0 \\ 0 & 0 & 0 & 0 \\ 0 & 0 & \frac{Y\dot{Y}}{N} & 0 \\ 0 & 0 & 0 & \frac{Y\dot{Y}}{N}\sin^2(\theta) \end{pmatrix}. \tag{18}$$

As mentioned before, we can use these data to compute the expansion scalar and shear and vorticity parameters as

$$\tilde{\theta} = 2\frac{\dot{Y}}{NY}, \tag{19}$$

$$\tilde{\sigma}^2 = 0, \tag{20}$$

$$\tilde{\omega}_{ab} = 0. \tag{21}$$

While quantities are simpler compared to the timelike case, we still need the equations of motion in order to be able to compute the expansion. The Raychaudhuri equation can be computed as before by using the Ricci tensor, as

$$\frac{d\theta}{d\lambda} = -\frac{2\dot{N}}{N^3}\frac{\dot{Y}}{Y} - \frac{2}{N^2}\frac{\dot{X}}{X}\frac{\dot{Y}}{Y} + \frac{2}{N^2}\frac{\ddot{Y}}{Y} - \frac{2}{N^2}\left(\frac{\dot{Y}}{Y}\right)^2. \tag{22}$$

3. Classical Schwarzschild Interior

3.1. Metric and Classical Hamiltonian

Before considering the quantum effects, let us first analyze the classical interior in the light of the expansion scalar and the Raychaudhuri equation. For this we need the metric of the interior and the classical Hamiltonian. Since crossing the event horizon of the Schwarzschild black hole results in change of causal nature (spacelike/timelike) of r, t, the metric of the interior can be obtained by switching $t \leftrightarrow r$ of the usual Schwarzschild metric as

$$ds^2 = -\left(\frac{2GM}{t} - 1\right)^{-1} dt^2 + \left(\frac{2GM}{t} - 1\right) dr^2 + t^2\left(d\theta^2 + \sin^2\theta d\phi^2\right). \tag{23}$$

Here and throughout the paper, t is the Schwarzschild time coordinate (in the exterior) which has a range $t \in (0, 2GM)$ in the interior. Such a metric is a special case of a Kantowski-Sachs cosmological spacetime that is given by the metric [67]

$$\begin{aligned} ds^2_{KS} =& -N(T)^2 dT^2 + g_{xx}(T)dx^2 + g_{\theta\theta}(T)d\theta^2 + g_{\phi\phi}(T)d\phi^2 \\ =& -d\tau^2 + g_{xx}(\tau)dx^2 + g_{\Omega\Omega}(\tau)d\Omega^2. \end{aligned} \tag{24}$$

Note that x here is not necessarily the radius r of the 2-spheres with area $A = 4\pi r^2$, but it can be chosen to be. Here $N(T)$ is the lapse function corresponding to a generic time, and τ is the proper time. The metric Equation (24) represents a cosmology with spatial homogeneous but anisotropic foliations.

To canonically analyze the model, one decomposes the spacetime into space and time by foliating spacetime into spatial hypersurfaces with constant coordinate time using the ADM method. This induces a spatial metric q_{ab} on the hypersurfaces. The classical Hamiltonian we will be working with is the one written in terms of Ashtekar–Barbero connection A^i_a, and its conjugate the densitized triad $\tilde{E}^a_i$. The Ashtekar–Barbero connection

$$A^i_a = \Gamma^i_a + \gamma K^i_a \tag{25}$$

is an $su(2)$ connection with i being an $su(2)$ index and a an spatial index. It is the sum of two terms. The hodge dual of the spin connection $\omega_a{}^{ij}$ denoted by $\Gamma^i_a = \frac{1}{2}\epsilon^i{}_{ij}\omega_a{}^{ij}$ where $\omega_a{}^{ij}$ associated with the symmetry under the Lorentz transformations, and the extrinsic curvature $K^i_a := \omega_a{}^{0i}$. The parameter γ is called the Barbero–Immirzi parameter which is a free parameter of the theory, and ϵ_{ijk} is the totally antisymmetric Levi-Civita symbol. The densitized triad is related to the spatial metric q_{ab} via

$$qq^{ab} = \delta^{ij}\tilde{E}^a_i\tilde{E}^b_j \tag{26}$$

with $q = \det(q_{ab})$. The full gravitational Hamiltonian constrain in terms of Ashtekar–Barbero connection and densitized triad is

$$H_{\text{full}} = \frac{1}{8\pi G}\int d^3x \frac{N}{\sqrt{\det|\tilde{E}|}}\left\{\epsilon_i^{jk} F^i_{ab}\tilde{E}^a_j\tilde{E}^b_k - 2\left(1+\gamma^2\right)K_{[a}{}^i K^j_{b]}\tilde{E}^a_i\tilde{E}^b_j\right\}, \tag{27}$$

Here, $F = dA + A\wedge A$ is the curvature of the Ashtekar–Barbero connection and N is the lapse function.

To obtain the classical Hamiltonian of the model, we take the above Hamiltonian constraint and reduce it by replacing the canonical variables with the ones adapted to the model,

$$A^i_a\tau_i dx^a = \frac{c}{L_0}\tau_3 dx + b\tau_2 d\theta - b\tau_1\sin\theta d\phi + \tau_3\cos\theta d\phi, \tag{28}$$

$$\tilde{E}^a_i\tau_i\partial_a = p_c\tau_3\sin\theta\partial_x + \frac{p_b}{L_0}\tau_2\sin\theta\partial_\theta - \frac{p_b}{L_0}\tau_1\partial_\phi. \tag{29}$$

Here b, c, p_b and p_c are functions that only depend on time, and $\tau_i = -i\sigma_i/2$ are a $su(2)$ basis satisfying $\left[\tau_i,\tau_j\right] = \epsilon_{ij}{}^k\tau_k$, with σ_i being the Pauli matrices. Substituting these into the full Hamiltonian of gravity written in Ashtekar connection variables, one obtains the symmetry reduced Hamiltonian constraint adapted to this model as [2]

$$H = -\frac{N\text{sgn}(p_c)}{2G\gamma^2}\left[2bc\sqrt{|p_c|} + \left(b^2+\gamma^2\right)\frac{p_b}{\sqrt{|p_c|}}\right], \tag{30}$$

while the diffeomorphism constraint vanishes identically due to homogenous nature of the model. This classical Hamiltonian is not different from other classical Hamiltonian since we have only changed the variables from metric to connection ones. The real difference comes about once we write Equation (27) in terms of holonomies instead of connection components.

Since the spatial hypersurfaces have a topology $\mathbb{R}\times\mathbb{S}^2$, the symplectic 2-form is

$$\Omega = \frac{1}{8\pi G\gamma}\int_{\mathbb{R}\times\mathbb{S}^2} d^3x\, dA^i_a(\mathbf{x})\wedge d\tilde{E}^a_i(\mathbf{y}). \tag{31}$$

However, the part of the integral over $\mathbb{R}$ diverges and we will not be able to obtain a kinematical structure, i.e., a Poisson bracket. To remedy this and since the model is homogeneous, one can restrict the range of integration in $\mathbb{R}$ to $\mathcal{I} = [0, L_0]$ and later take the limit $L_0\to\infty$. This we symplectic 2-form becomes

$$\begin{aligned}\Omega =& \frac{1}{8\pi G\gamma}\int_{\mathcal{I}\times\mathbb{S}^2} d^3x\, dA^i_a(\mathbf{x})\wedge d\tilde{E}^a_i(\mathbf{y})\\ =& \frac{1}{2G\gamma}(dc\wedge dp_c + 2db\wedge dp_b),\end{aligned} \tag{32}$$

and consequently the fundamental Poisson brackets are

$$\{c, p_c\} = 2G\gamma, \qquad \{b, p_b\} = G\gamma. \tag{33}$$

Using Equations (24), (26), and (29), one obtains

$$g_{xx}(T) = \frac{p_b(T)^2}{L_0^2 p_c(T)}, \tag{34}$$

$$g_{\theta\theta}(T) = \frac{g_{\phi\phi}(T)}{\sin^2(\theta)} = g_{\Omega\Omega}(T) = p_c(T). \tag{35}$$

These results correspond to a generic lapse function associated with a generic time coordinate T. If in the above we choose the time and the lapse function to be the Schwarzschild time t and its lapse respectively, and then compare the results with Equation (23), we obtain

$$N(t) = \left(\frac{2GM}{t} - 1\right)^{-\frac{1}{2}}, \tag{36}$$

$$g_{xx}(t) = \frac{p_b(t)^2}{L_0^2 p_c(t)} = \left(\frac{2GM}{t} - 1\right), \tag{37}$$

$$g_{\theta\theta}(T) = \frac{g_{\phi\phi}(T)}{\sin^2(\theta)} = g_{\Omega\Omega}(T) = p_c(t) = t^2. \tag{38}$$

This shows that

$$p_b = 0, \qquad p_c = 4G^2M^2, \qquad \text{on the horizon } t = 2GM, \tag{39}$$

$$p_b \to 0, \qquad p_c \to 0, \qquad \text{at the singularity } t \to 0. \tag{40}$$

3.2. Dynamics, Expansion Scalar and Raychaudhuri Equation

3.2.1. Generic θ and $\frac{d\theta}{d\tau}$

Comparing the metric Equation (3) with Equations (34) and (35), and also using Equation (47), we notice

$$X^2 = \frac{p_b(T)^2}{L_0^2 p_c(T)}, \tag{41}$$

$$Y^2 = p_c(T). \tag{42}$$

Replacing Equations (41) and (42) in the timelike expansion Equation (10) yields

$$\theta = \pm\left(\frac{\dot{p}_b}{N p_b} + \frac{\dot{p}_c}{2N p_c}\right). \tag{43}$$

Notice that the above results are generic for any lapse and its associated time and also valid in both classical and effective regimes. The difference between these two regimes comes later due to the different equations of motion which we will replace in the above expansion formula. For the null case, we again replace Equations (41) and (42) into Equation (19) to obtain

$$\theta = \pm\frac{\dot{p}_c}{N p_c}. \tag{44}$$

Using the above expressions for X, Y, N in the timelike Raychaudhuri Equation (13), we obtain

$$\frac{d\theta}{d\tau} = \frac{1}{N^2}\left(-\frac{\dot{N}\dot{p}_b}{N p_b} - \frac{\dot{N}\dot{p}_c}{2N p_c} + \frac{\ddot{p}_b}{p_b} - \frac{\dot{p}_b^2}{p_b^2} + \frac{\ddot{p}_c}{2p_c} - \frac{\dot{p}_c^2}{2p_c^2}\right). \tag{45}$$

The same method for the null Raychaudhuri Equation (22) yields

$$\frac{d\theta}{d\lambda} = \frac{1}{N^2}\left(-\frac{\dot{N}\dot{p}_c}{N p_c} - \frac{\dot{p}_b\dot{p}_c}{p_b p_c} + \frac{\ddot{p}_c}{p_c} - \frac{\dot{p}_c^2}{2p_c^2}\right). \tag{46}$$

These last two expressions are also generic results and are valid for any time, lapse, and in both classical and effective regimes.

Notice that the fiducial parameter L_0 is not explicitly present neither in θ nor in $\frac{d\theta}{d\tau}$ above. Of course, it is hidden in the classical solutions of p_b and c (see below), but wherever we have a term such as $\frac{\dot{p}_b}{p_b}$ or $\frac{\ddot{p}_b}{p_b}$, etc., L_0 will be canceled out. Hence the above physical expressions are independent of L_0 as they should be.

3.2.2. Classical Dynamics

In order to obtain the explicit expressions for θ and $\frac{d\theta}{d\tau}$ from above relations, we need the equations of motion and their solutions. To this end we choose a lapse function

$$N(T) = \frac{\gamma \operatorname{sgn}(p_c)\sqrt{|p_c(T)|}}{b(T)}. \tag{47}$$

The advantage of this lapse function is that the equations of motion of c, p_c decouple from those of b, p_b and it makes it possible to solve them. Replacing this lapse function into Equation (30) yields

$$H = -\frac{1}{2G\gamma}\left[\left(b^2+\gamma^2\right)\frac{p_b}{b} + 2cp_c\right]. \tag{48}$$

Using this Hamiltonian together with the Poisson brackets Equation (33), we can obtain the classical equations of motion

$$\frac{db}{dT} = \{b, H\} = -\frac{1}{2}\left(b + \frac{\gamma^2}{b}\right), \tag{49}$$

$$\frac{dp_b}{dT} = \{p_b, H\} = \frac{p_b}{2}\left(1 - \frac{\gamma^2}{b^2}\right). \tag{50}$$

$$\frac{dc}{dT} = \{c, H\} = -2c, \tag{51}$$

$$\frac{dp_c}{dT} = \{p_c, H\} = 2p_c. \tag{52}$$

These equations should be supplemented by the weakly vanishing ($\approx$0) of the Hamiltonian constraint Equation (48),

$$\left(b^2+\gamma^2\right)\frac{p_b}{b} + 2cp_c \approx 0. \tag{53}$$

This system can be solved to yield the solutions in generic time T. In order to write the solutions in Schwarzschild time t, one compares the form of $p_c(T)$ with its Schwarzschild couterpart $p_c = t^2$ and this reveals that to go from T to t, we should make a transformation of the form $T = \ln(t)$. Doing that we obtain

$$b(t) = \pm\,\gamma\sqrt{\frac{2GM}{t} - 1}, \tag{54}$$

$$p_b(t) = L_0 t\sqrt{\frac{2GM}{t} - 1}, \tag{55}$$

$$c(t) = \mp\,\frac{\gamma G M L_0}{t^2}, \tag{56}$$

$$p_c(t) = t^2, \tag{57}$$

where the constants of integration in these solutions are fixed using Equations (37)–(39).

3.2.3. Classical θ and $\frac{d\theta}{d\tau}$: Timelike Congruence

To obtain the expressions for expansion and Raychaudhuri equation for a timelike congruence, we replace Equations (49)–(52) and Equation (47) in Equation (43) to

$$\theta = \pm\frac{1}{2\sqrt{p_c}}\left(\frac{3b}{\gamma} - \frac{\gamma}{b}\right) = \pm\frac{-2t + 3GM}{t^2\sqrt{\frac{2GM}{t} - 1}}. \tag{58}$$

where in the last step to get an explicit expression in terms of the Schwarzschild time t we have made use of Equations (54)–(57). The $\pm$ corresponds to ingoing vs. outgoing

geodesics. Since in the interior $t \leq 2GM$, from $\frac{3}{2}GM \leq t \leq 2GM$, the ingoing (negative branch) of the expansion is positive while for $t < \frac{3}{2}GM$, this branch becomes negative and continues to become more negative until at $t \to 0$ it goes to $\theta \to -\infty$.

Notice that the above expression in terms of b, p_c contains three terms that are all negative (since p_c is always positive as is seen from Equation (57)). This guarantees that there will be a caustic point at the region where classically we identify as the singularity. The plots of expansion and Raychaudhuri equation are in Schwrazschild time are presented in Figure 1. It is clear from this plot that both of them diverge at the singularity at $t \to 0$.

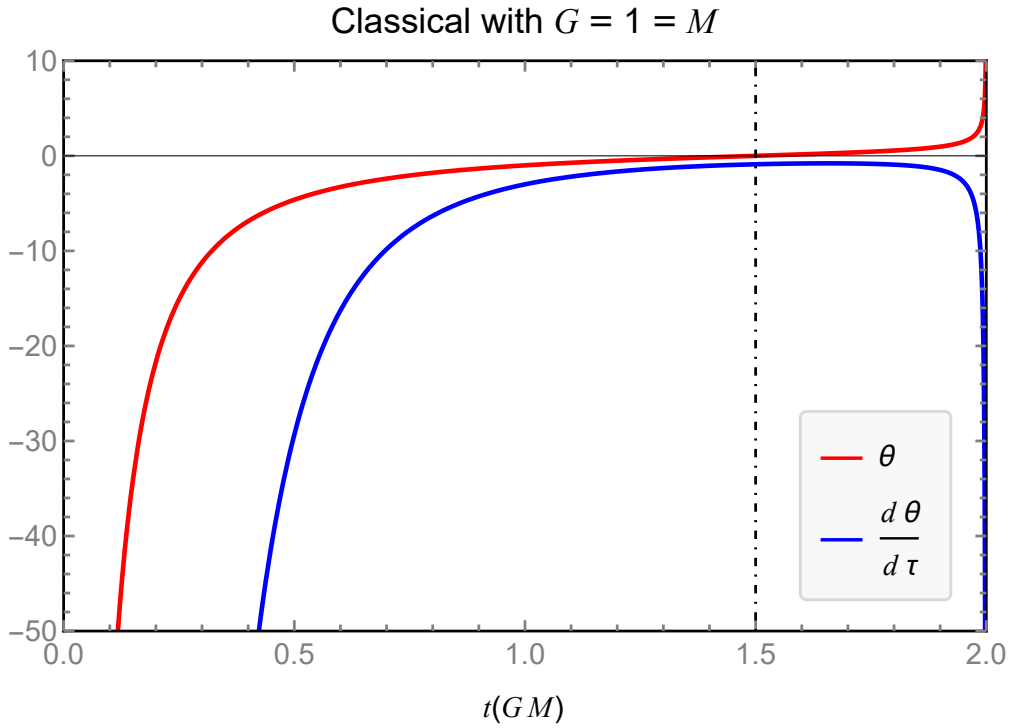

Figure 1. Classical timelike θ and $\frac{d\theta}{d\tau}$ diverge as we approach $t \to 0$. The divergence at the horizon is due to the choice of Schwarzschild coordinate system. The dashed line is where θ changes sign.

We can use Equations (47), (49)–(52) and (54)–(57) in the same way in Equation (45) to obtain

$$\frac{d\theta}{d\tau} = -\frac{1}{2p_c}\left(1 + \frac{9b^2}{2\gamma^2} + \frac{\gamma^2}{2b^2}\right) = \frac{-2t^2 + 8GMt - 9G^2M^2}{(2GM - t)t^3}. \tag{59}$$

3.2.4. Classical θ and $\frac{d\theta}{d\tau}$: Null Congruence

The expression Equation (19) for the null expansion is actually simpler than its timelike counterpart. As in the previous section, once we replace Equations (49)–(52) and Equation (47) into Equation (19) we get

$$\theta = \pm\frac{2b}{\gamma\sqrt{p_c}} = \pm\frac{2}{t}\sqrt{\frac{2GM}{t} - 1}. \tag{60}$$

where once again in the last step we have used Equations (54)–(57). Here, as opposed to the timelike case Equation (58), θ remain negative everywhere in the interior where $t < 2GM$ and there are no roots to the expansion scalar. This makes sense since usually the existence of roots of the expansion scalar points to the existence of a horizon. Furthermore, the ingoing branch of the expansion scalar goes to $\theta \to -\infty$ as $t \to 0$.

To obtain the form of the Raychaudhuri equation, we use Equations (47), (49)–(52), and Equations (54)–(57) in Equation (46) to obtain

$$\frac{d\theta}{d\lambda} = -\frac{2b^2}{\gamma^2 p_c} = -\frac{2}{t^2}\left(\frac{2GM}{t} - 1\right), \tag{61}$$

which clearly is always negative in the interior. Since θ is negative at least at one point in the interior and $\tilde{\omega}_{ab} = 0$, the theorem we mentioned in Appendix A guarantees the existence of caustic point(s) in the interior, which from the above is seen to be at $t \to 0$. This can also simply be deduced by noting that both θ and $\frac{d\theta}{d\tau}$ are always negative in the interior and tend to $-\infty$ as $t \to 0$. This behavior can be seen in Figure 2.

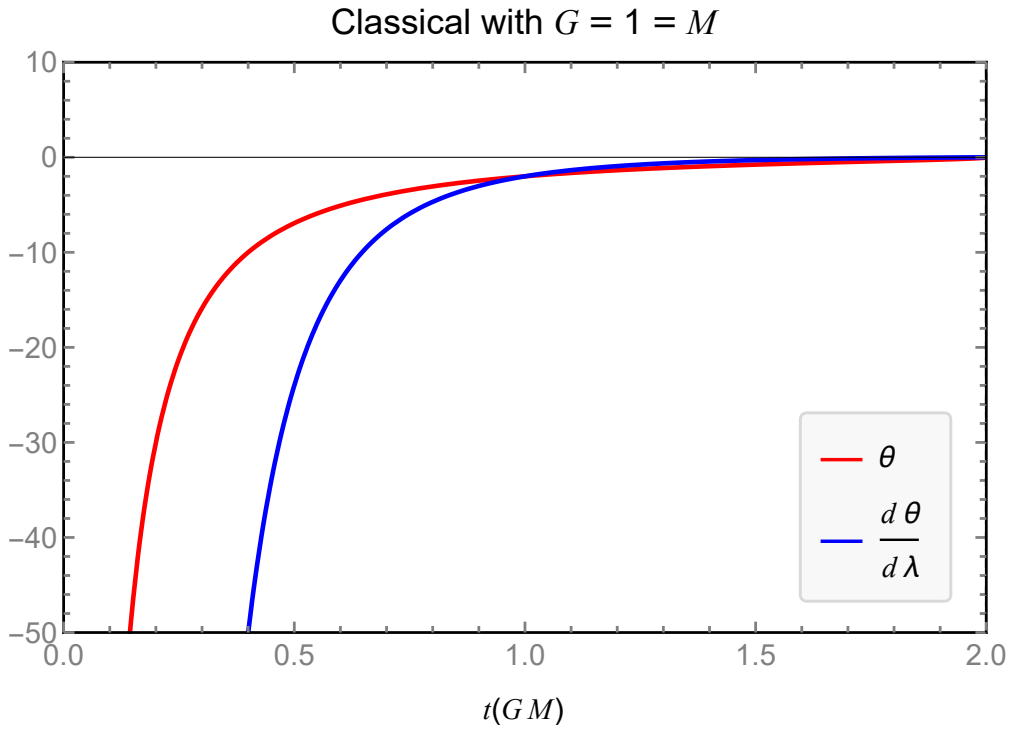

Figure 2. Classical null θ and $\frac{d\theta}{d\lambda}$ diverge as we approach $t \to 0$. Notice that θ always remains negative and has no roots.

3.2.5. Classical Kretschmann Scalar

In our variables the Kretchammn scalar becomes

$$K = \frac{12\left(b^2 + \gamma^2\right)^2}{\gamma^4 p_c^2} \tag{62}$$

which in terms of the Schwarzschild time turns out to be

$$K = \frac{48G^2M^2}{t^6} \tag{63}$$

and unsurprisingly it diverges at $t \to 0$ or equivalently at $p_c \to 0$. Notice that p_c is the radius of the infalling 2-spheres as can be seen from Equation (57).

4. Effective Schwarzschild Interior

The main idea in this section is to find the modified equations of motion of the interior, and use them to compute the effective expansion and Raychaudhuri equation for null and timelike cases. We consider two models, one coming from loop quantum gravity (LQG) and the other one from generalized uncertainty principle (GUP).

4.1. Loop Quantum Gravity

In LQG, the configuration variable is not the connection, but the holonomy of the connection $h_\xi[A]$, .i.e., path-ordered exponential of the connection A_a^i along some curves ξ in space. The canonically conjugate momenta to this variable is the smeared flux of the densitized triad over a two dimensional spatial surface. As a consequence, to derive a quantum Hamiltonian, one goes back to Eqaution (27) and writes the curvatures F_{ab}^i in terms of holonomies instead of the connection. Once this expression is derived classically, then one quantizes the Hamiltonian on a suitable Hilbert space. On this Hilbert space, only the operators $\hat{h}_\xi[A]$ exists. There is no operator corresponding to A. As a consequence the Hilbert space of LQG is unitarily inequivalent to the usual Schrodinger representation. Another type of quantization which mimics LQG quantization which is usually used is called polymer quantization. This quantiztion introduces parameters into the theory called polymer scales that set the minimal scale of the model. Close to this scale quantum effects become important. In case of the present model such a polymer quantization leads to polymer scales μ_b, μ_c associated with the radial and angular minimum scales [2,6,13,68].

After applying the polymer quantization to the model and obtaining the quantum Hamiltonian as mentioned above, one finds an effective Hamiltonian by either using a path integral approach, or by acting the quantum Hamiltonian on suitable states [34,42–46,69]. These methods will lead to an effective Hamiltonian that can also be heuristically obtained by replacing

$$b \to \frac{\sin(\mu_b b)}{\mu_b}, \tag{64}$$

$$c \to \frac{\sin(\mu_c c)}{\mu_c} \tag{65}$$

in the classical Hamiltonian which yields an effective Hamiltonian constraint,

$$H_{\text{eff}}^{(N)} = -\frac{N}{2G\gamma^2}\left[\left(\frac{\sin^2(\mu_b b)}{\mu_b^2}+\gamma^2\right)\frac{p_b}{\sqrt{p_c}} + 2\frac{\sin(\mu_b b)}{\mu_b}\frac{\sin(\mu_c c)}{\mu_c}\sqrt{p_c}\right]. \tag{66}$$

In LQG, there exist two general schemes regarding these μ parameters. In one, called the μ_0 scheme, μ parameters are considered to be constants [2,24,30,70]. Applying such a scheme to isotropic and Bianchi-I cosmological models, however, has shown to lead to incorrect semiclassical limit. To remedy this and other issues regarding the appearance of large quantum effects at the horizon or dependence of physical quantities on fiducial variables, new schemes referred to as the $\bar{\mu}$ scheme or "improved dynamics" have been proposed in which μ parameters depend on canonical variables [5,13,49,68]. This scheme is itself divided into various different ways of expressing the dependence of μ parameters on canonical variables. In addition, new μ_0 schemes have also been put forward (e.g., Refs. [6,26]) with the intent of resolving the aforementioned issues. In case of the Schwarzschild interior due to lack of matter content, it is not clear which scheme does not lead to the correct semiclassical limit. Hence for completeness, in this paper, we will study the modifications to the Raychaudhuri equation in the constant μ scheme, which here we call the $\mathring{\mu}$ scheme, as well as in two of the most common improved schemes, which we denote by $\bar{\mu}$ and $\bar{\mu}'$ schemes. These schemes were originally introduced in [71,72]. In the $\mathring{\mu}$ scheme, the polymer parameter is taken to be a constant, while in the $\bar{\mu}$ and $\bar{\mu}'$ schemes, this parameter depends on the canonical momenta, but this dependence is difference for each of the last two schemes, as we will see in the following sections.

In order to be able to find the deviations from the classical behavior, we need to use the same lapse as we did in the classical part. Using Equation (64), the lapse Equation (47) becomes (assuming $p_c \geq 0$)

$$N = \frac{\gamma\mu_b\sqrt{p_c}}{\sin(\mu_b b)}. \tag{67}$$

Using this in Equation (66) yields

$$H_{\text{eff}} = -\frac{1}{2\gamma G}\left[p_b\left[\frac{\sin(\mu_b b)}{\mu_b} + \gamma^2\frac{\mu_b}{\sin(\mu_b b)}\right] + 2p_c\frac{\sin(\mu_c c)}{\mu_c}\right]. \tag{68}$$

The parameters μ_b, μ_c here are written in a generic form meaning that they can be either $\mathring{\mu}$, $\bar{\mu}$ or $\bar{\mu}'$ depending on the scheme we are considering. Furthermore, note that both Equations (66) and (68) reduce to their classical counterparts Equations (30) and (48) respectively for μ_b, $\mu_c \to 0$, as expected.

4.1.1. $\mathring{\mu}$ Scheme

As mentioned before, in this scheme, one assumes that the polymer or minimal scales $\mathring{\mu}_b$, $\mathring{\mu}_c$ are constants. The equations of motion corresponding to Equation (68) become

$$\frac{db}{dT} = \{b, H_{\text{eff}}\} = -\frac{1}{2}\left[\frac{\sin(\mathring{\mu}_b b)}{\mathring{\mu}_b} + \gamma^2\frac{\mathring{\mu}_b}{\sin(\mathring{\mu}_b b)}\right], \tag{69}$$

$$\frac{dp_b}{dT} = \{p_b, H_{\text{eff}}\} = \frac{1}{2}p_b\cos(\mathring{\mu}_b b)\left[1 - \gamma^2\frac{\mathring{\mu}_b^2}{\sin^2(\mathring{\mu}_b b)}\right], \tag{70}$$

$$\frac{dc}{dT} = \{c, H_{\text{eff}}\} = -2\frac{\sin(\mathring{\mu}_c c)}{\mathring{\mu}_c}, \tag{71}$$

$$\frac{dp_c}{dT} = \{p_c, H_{\text{eff}}\} = 2p_c\cos(\mathring{\mu}_c c). \tag{72}$$

Notice that the $\mathring{\mu}_b \to 0$ and $\mathring{\mu}_c \to 0$ limit of these equations corresponds to the classical equations of motion. The solutions to these equations in terms of the Schwarzschild time t (after a transformation $T = \ln(t)$) and finding the integration constants by matching the limit $\mathring{\mu}_b$, $\mathring{\mu}_c \to 0$ to classical solutions, are given by

$$b(t) = \frac{\cos^{-1}\left[\sqrt{1+\gamma^2\mathring{\mu}_b^2}\tanh\left(\sqrt{1+\gamma^2\mathring{\mu}_b^2}\ln\left[\frac{2\sqrt{\frac{t}{2GM}}}{\gamma\mathring{\mu}_b}\right]\right)\right]}{\mathring{\mu}_b}, \tag{73}$$

$$p_b(t) = \frac{\gamma\mathring{\mu}_b L_0 GM\left(\frac{\gamma^2\mathring{\mu}_c^2 L_0^2 G^2M^2}{4t^2} + t^2\right)\sqrt{1-\left(1+\gamma^2\mathring{\mu}_b^2\right)\tanh^2\left(\sqrt{\gamma^2\mathring{\mu}_b^2+1}\ln\left[\frac{2\sqrt{\frac{t}{2GM}}}{\gamma\mathring{\mu}_b}\right]\right)}}{t^2\sqrt{\frac{\gamma^2\mathring{\mu}_c^2 L_0^2 G^2M^2}{4t^4}+1}\left(\gamma^2\mathring{\mu}_b^2 - \left(1+\gamma^2\mathring{\mu}_b^2\right)\tanh^2\left(\sqrt{1+\gamma^2\mathring{\mu}_b^2}\ln\left[\frac{2\sqrt{\frac{t}{2GM}}}{\gamma\mathring{\mu}_b}\right]\right)+1\right)}, \tag{74}$$

$$c(t) = -\frac{\tan^{-1}\left(\frac{\gamma\mathring{\mu}_c L_0 GM}{2t^2}\right)}{\mathring{\mu}_c}, \tag{75}$$

$$p_c(t) = \frac{\gamma^2\mathring{\mu}_c^2 L_0^2 G^2M^2}{4t^2} + t^2. \tag{76}$$

Since p_c represents the radius of two spheres, it is interesting to see that it never reaches zero. This is the first sign that the singularity is resolved as we will see in the following. The plot of the behavior of these solutions can be seen in Figure 3. The timelike expansion Equation (43) in this case becomes

$$\theta^{\text{TL}}_{(\mathring{\mu})} = \pm\frac{1}{\gamma\sqrt{p_c}}\left[\frac{\sin(\mathring{\mu}_b b)}{\mathring{\mu}_b}\cos(\mathring{\mu}_c c) - \frac{\gamma^2}{2}\frac{\mathring{\mu}_b}{\sin(\mathring{\mu}_b b)}\cos(\mathring{\mu}_b b) + \frac{\sin(2\mathring{\mu}_b b)}{2\mathring{\mu}_b}\right]. \tag{77}$$

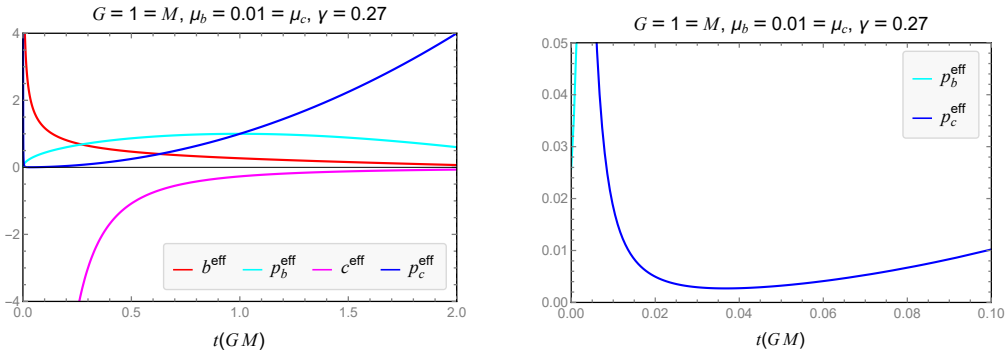

(**a**) (**b**)

Figure 3. Solutions of the EoM of the $\mathring{\mu}$ case. (**a**) Solutions to the equations of motion in $\mathring{\mu}$ case as a function of the Schwarzschild time t. (**b**) Close up of the EoM of p_c close to $t = 0$. We can see that p_c never vanishes.

Up to the second order in $\mathring{\mu}_b$, $\mathring{\mu}_c$, the negative branch of this expression can be written as

$$\theta^{\mathrm{TL}}_{(\mathring{\mu})} = -\frac{1}{2\sqrt{p_c}}\left(\frac{3b}{\gamma} - \frac{\gamma}{b} + b\gamma\left(\frac{1}{3} - \frac{b^2}{\gamma^2}\right)\mathring{\mu}_b^2 - \frac{b}{\gamma}c^2\mathring{\mu}_c^2\right) + \mathcal{O}\left(\mathring{\mu}^4\right). \tag{78}$$

The first two terms are the classical ones that contribute to a negative expansion or focusing. The last term, which is an effective term, is always positive and given the behavior of b, c in this scheme seen from Equations (73) and (75), it becomes very large as $t \to 0$. The third term is also an effective term and becomes positive for $b^2 > \frac{\gamma^2}{3}$, which is indeed the case from the solution Equation (73). These two effective terms take over close to where the classical singularity used to be and stop the congruence from infinitely focusing. In fact the full nonperturbative plot Figure 4, obtained by replacing the solutions Equations (73)–(76) into Equation (77), reveals that the effective terms perfectly cancel the classical focusing terms such that $\theta^{\mathrm{TL}}_{(\mathring{\mu})}$ becomes zero at $t = 0$.

The Raychaudhuri Equation (45) in this case also turns out to be

$$\begin{aligned}\frac{d\theta^{\mathrm{TL}}_{(\mathring{\mu})}}{d\tau} =& \frac{1}{4\gamma^2 p_c}\left\{-\gamma^2 + \frac{5}{4\mathring{\mu}_b^2} + \frac{6\sin^2(\mathring{\mu}_b b)}{\mathring{\mu}_b^2}\left[\sin^2(\mathring{\mu}_c c) - \cos^2(\mathring{\mu}_c c)\right] - \frac{3\cos^2(\mathring{\mu}_b b)}{2\mathring{\mu}_b^2}\right.\\ &+ \frac{7\sin^4(\mathring{\mu}_b b)}{4\mathring{\mu}_b^2} + \frac{\cos^4(\mathring{\mu}_b b)}{4\mathring{\mu}_b^2} - \frac{4\sin^2(\mathring{\mu}_b b)}{\mathring{\mu}_b^2}\cos(\mathring{\mu}_b b)\cos(\mathring{\mu}_c c)\\ &\left.-\gamma^4\frac{\mathring{\mu}_b^2}{\sin^2(\mathring{\mu}_b b)} + \gamma^2\left[\sin^2(\mathring{\mu}_b b) - \cos^2(\mathring{\mu}_b b)\right]\right\}.\end{aligned} \tag{79}$$

Once again we see that perturbatively

$$\frac{d\theta^{\mathrm{TL}}_{(\mathring{\mu})}}{d\tau} \approx -\frac{1}{2p_c}\left(1 + \frac{9b^2}{2\gamma^2} + \frac{\gamma^2}{2b^2} - \left(b^2 + \frac{7b^4}{2\gamma^2} - \frac{\gamma^2}{6}\right)\mathring{\mu}_b^2 - \frac{7b^2c^2}{\gamma^2}\mathring{\mu}_c^2\right) + \mathcal{O}\left(\mathring{\mu}^4\right). \tag{80}$$

We see that the first three terms are the classical ones leading to focusing. The terms proportional to $\mathring{\mu}_b^2$ are all positive contributing to defocusing except the term $\frac{\gamma^2}{6}$ which is small and close to $t \to 0$ is much smaller that the other two terms. The term proportional to $\mathring{\mu}_c^2$ is always positive. These effective terms take over close to $t \to 0$ and stop focusing of the congruence. The full nonperturbative behavior of $\frac{d\theta^{\mathrm{TL}}_{(\mathring{\mu})}}{d\tau}$ can be derived numerically by replacing (73)–(76) into (79). It is plotted in Figure 4. It is seen that $\frac{d\theta^{\mathrm{TL}}_{(\mathring{\mu})}}{d\tau}$ becomes quite large and positive close to $t \to 0$, then dips a little bit below zero and the goes to zero at $t = 0$.

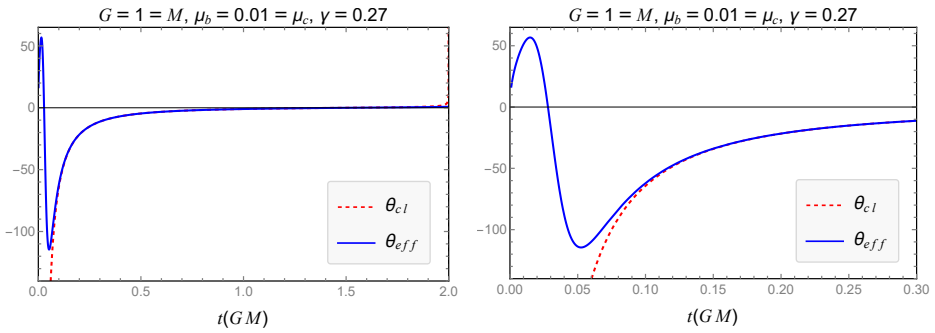

(**a**)

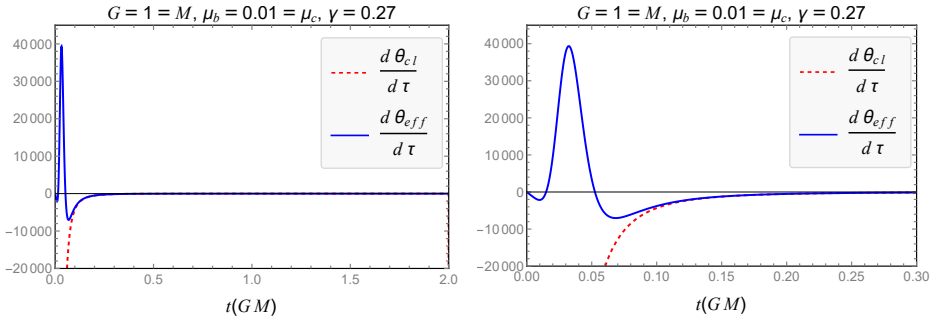

(**b**)

Figure 4. $\theta^{\mathrm{TL}}_{(\mathring{\mu})}$ and $\frac{d\theta^{\mathrm{TL}}_{(\mathring{\mu})}}{d\tau}$. (**a**) Left: Classical vs. timlike θ in the $\mathring{\mu}$ scheme as a function of the Schwarzschild time t. The effective expansion $\theta^{\mathrm{TL}}_{(\mathring{\mu})}$ goes to zero as $t \to 0$. Right: Close up of the left figure close to $t = 0$. (**b**) Left: Classical vs. timlike $\frac{d\theta}{d\tau}$ in the $\mathring{\mu}$ scheme as a function of the Schwarzschild time t. The effective $\frac{d\theta^{\mathrm{TL}}_{(\mathring{\mu})}}{d\tau}$ goes to zero as $t \to 0$. Right: Close up of the left figure close to $t = 0$.

Hence, a common theme in Figure 4 is that both $\theta^{\mathrm{TL}}_{(\mathring{\mu})}$ and $\frac{d\theta^{\mathrm{TL}}_{(\mathring{\mu})}}{d\tau}$ become zero as $t \to 0$, and neither of them ever blows up anywhere inside the black hole. This is a clear proof that the singularity is resolved. Furthermore, it can be seen that the effective and classical expansion and Raychaudhuri equation match very well far from the region used to be the singularity at $t = 0$. However, close to this region, quantum effects starts to take over and turn the curves around, stopping them from blowing up.

Null expansion and Raychaudhuri equations have nicer expressions. For the null expansion from Equations (44), (67), and (69)–(72) we obtain

$$\theta^{\mathrm{NL}}_{(\mathring{\mu})} = \pm \frac{2}{\gamma\sqrt{p_c}} \frac{\sin(\mathring{\mu}_b b)}{\mu_b} \cos(\mathring{\mu}_c c), \tag{81}$$

whose negative branch for small $\mathring{\mu}_b$, $\mathring{\mu}_c$ is

$$\theta^{\mathrm{NL}}_{(\mathring{\mu})} = \frac{1}{\gamma\sqrt{p_c}} \left(-2b + \frac{b^3}{3}\mathring{\mu}_b^2 + bc^2\mathring{\mu}_c^2 \right) + \mathcal{O}\left(\mathring{\mu}^4\right). \tag{82}$$

The first term is the classical term and while it is negative, contributing to the focusing, the other terms that are effective are always positive given the solutions Equations (73)–(76). They actually take over and stop the focusing of the congruence. The corresponding nonperturbative behavior is depicted in Figure 5, where it is seen that the expansion stops, turns around and reaches zero at $t = 0$.

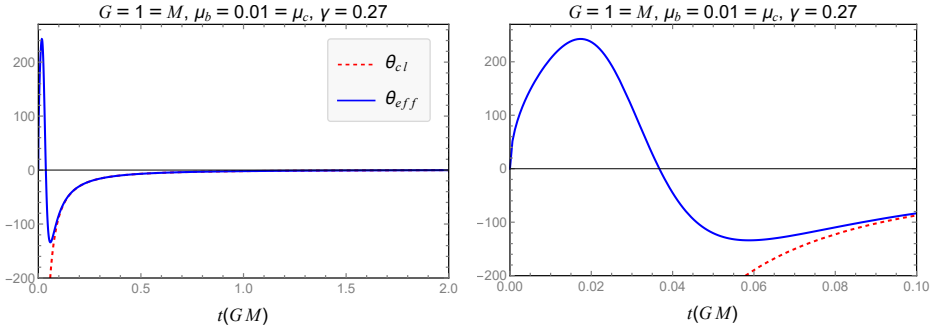

(**a**)

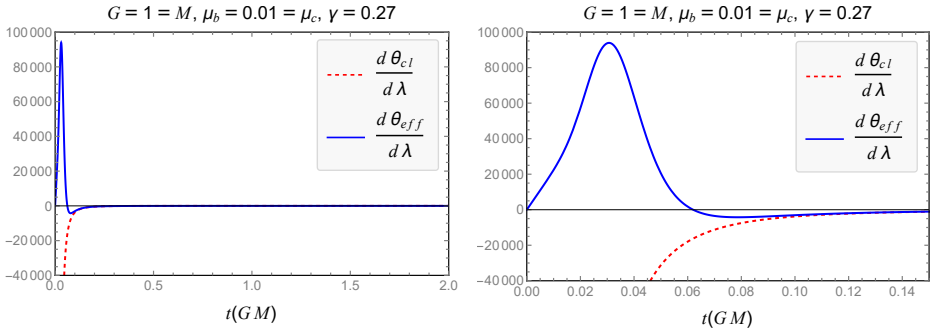

(**b**)

Figure 5. $\theta^{\rm NL}_{(\mathring{\mu})}$ and $\frac{d\theta^{\rm NL}_{(\mathring{\mu})}}{d\lambda}$. (**a**) Left: Classical vs. null θ in the $\mathring{\mu}$ scheme as a function of the Schwarzschild time t. The effective expansion $\theta^{\rm NL}_{(\mathring{\mu})}$ goes to zero as $t \to 0$. Right: Close up of the left figure close to $t = 0$. (**b**) Left: Classical vs. null $\frac{d\theta}{d\lambda}$ in the $\mathring{\mu}$ scheme as a function of the Schwarzschild time t. The effective $\frac{d\theta^{\rm NL}_{(\mathring{\mu})}}{d\lambda}$ goes to zero as $t \to 0$. Right: Close up of the left figure close to $t = 0$.

We can also derive an expression for the Raychaudhuri equation in this null case. Using Equations (67) and (69)–(72) in Equation (46) yields

$$\frac{d\theta^{\rm NL}_{(\mathring{\mu})}}{d\lambda} = \frac{2}{\gamma^2 p_c}\frac{\sin^2(\mathring{\mu}_b b)}{\mathring{\mu}_b^2}\left[2\sin^2(\mathring{\mu}_c c) - \cos(\mathring{\mu}_b b)\cos(\mathring{\mu}_b c)\right], \tag{83}$$

which, if Taylor expanded for small $\mathring{\mu}_b$, $\mathring{\mu}_c$ yields

$$\frac{d\theta^{\rm NL}_{(\mathring{\mu})}}{d\lambda} \approx \frac{1}{\gamma^2 p_c}\left(-2b^2 + \frac{5b^4}{3}\mathring{\mu}_b^2 + 5b^2c^2\mathring{\mu}_c^2\right) + \mathcal{O}\left(\mathring{\mu}^4\right). \tag{84}$$

The effective terms are both positive and based on our previous discussion, become very large close to $t = 0$. In this case too, the full nonperturbative solution depicted in Figure 5 shows that $\frac{d\theta^{\rm NL}_{(\mathring{\mu})}}{d\lambda}$ becomes positive close to $t = 0$ before vanishing at $t = 0$.

We can also look at the Kretschmann scalar to confirm the resolution of the singularity in the effective regime. The expression for the Kretschmann scalar K in terms of the canonical variables for $\mathring{\mu}$ case is quite large and we do not write it down here. However, we can first look at its terms up to the second order in $\mathring{\mu}_b$, $\mathring{\mu}_c$,

$$K = \frac{2}{\gamma^2 p_c^2}\left[12b^2 + \frac{6b^4}{\gamma^2} + 6\gamma^2 - \mathring{\mu}_b^2\left(\frac{b^6}{\gamma^2} + 3b^4 + 3\gamma^2 b^2 + \gamma^4\right)\right] + \mathcal{O}\left(\mathring{\mu}^4\right). \tag{85}$$

Interestingly, while the classical terms (the first three terms) are always positive, the effective terms proportional to $\mathring{\mu}_b^2$ are all negative and counter the classical terms. These terms become large close to the region used to be the singularity and stop K from diverging.

In fact K becomes zero at $t = 0$. This can be checked from the full numerical nonperturbative behavior of K as a function of the Schwarzschild time t in Figure 6. As we can see, K never diverges in the interior, and although it has a large increase close to $t = 0$, the quantum effects become so large in that region that turn the curve back towards zero, and we obtain $K \to 0$ as $t \to 0$. This together with the above results regarding the expansion scalar and the Raychaudhuri equation definitely prove that the singularity is removed in this model.

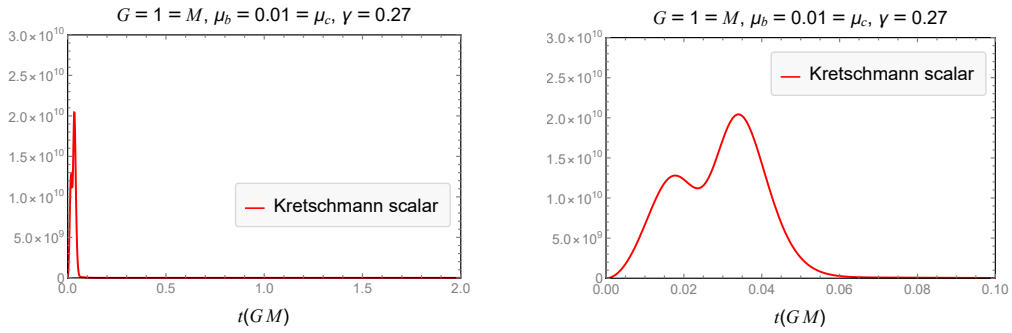

(**a**) (**b**)

Figure 6. K in the $\mathring{\mu}$ case. (**a**) The Kretschmann scalar K for the $\mathring{\mu}$ case as a function of the Schwarzschild time t. (**b**) Close up of K close to $t = 0$. It is seen that K remains finite everywhere in the interior and vanishes for $t = 0$.

4.1.2. $\bar{\mu}$ Scheme

In this scheme $\bar{\mu}_b$, $\bar{\mu}_c$ are assumed to depend on the triad components as

$$\bar{\mu}_b = \sqrt{\frac{\Delta}{p_b}}, \tag{86}$$

$$\bar{\mu}_c = \sqrt{\frac{\Delta}{p_c}}, \tag{87}$$

where Δ is related to the minimum area in loop quantum gravity. Using the same lapse as Equation (67) but keeping in mind the above dependence of $\bar{\mu}_b$, $\bar{\mu}_c$, one can easily obtain the equations of motion as

$$\frac{db}{dT} = \frac{1}{4}\left(b\cos(\bar{\mu}_b b) - 3\frac{\sin(\bar{\mu}_b b)}{\bar{\mu}_b} - \gamma^2 \frac{\bar{\mu}_b}{\sin(\bar{\mu}_b b)}\left[1 + b\cos(\bar{\mu}_b b)\frac{\bar{\mu}_b}{\sin(\bar{\mu}_b b)}\right]\right), \tag{88}$$

$$\frac{dp_b}{dT} = \frac{1}{2}p_b\cos(\bar{\mu}_b b)\left[1 - \gamma^2\frac{\bar{\mu}_b^2}{\sin^2(\bar{\mu}_b b)}\right], \tag{89}$$

$$\frac{dc}{dT} = c\cos(\bar{\mu}_c c) - 3\frac{\sin(\bar{\mu}_c c)}{\bar{\mu}_c}, \tag{90}$$

$$\frac{dp_c}{dT} = 2p_c\cos(\bar{\mu}_c c). \tag{91}$$

The solutions to these equations can be derived numerically by demanding the solutions match the classical ones very close to the horizon at $t = 2GM$. These are plotted in Figure 7.

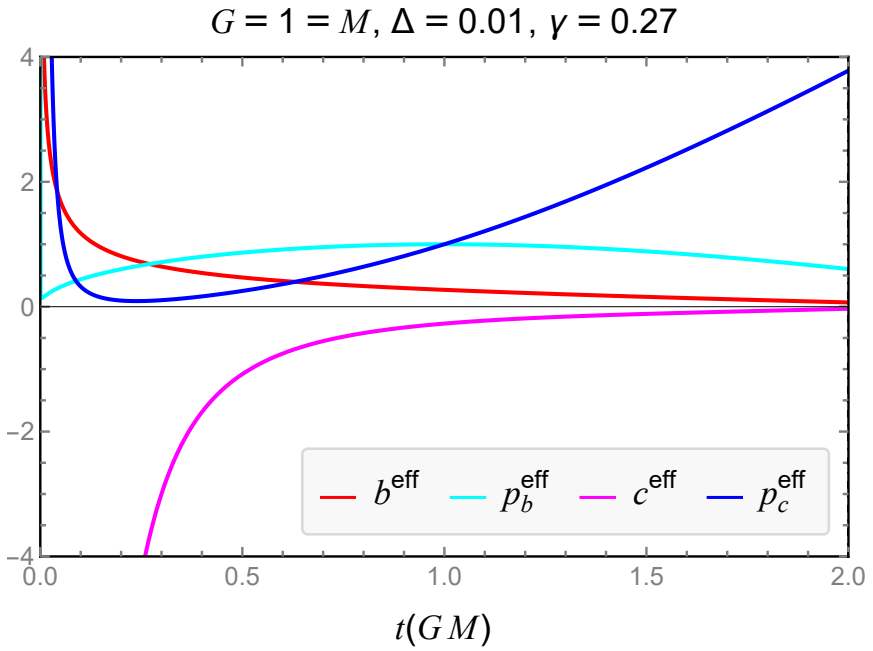

Figure 7. Solutions to the equations of motion in the $\bar{\mu}$ case as a function of the Schwarzschild time t. Once again, p_c never vanishes.

Analytical solutions to these equations are hard to obtain, but one can numerically solve them. The constants of integration are determined by matching these solution with the classical ones very close to the horizon for $\Delta \to 0$. The expressions for timelike $\theta^{\mathrm{TL}}_{(\bar{\mu})}$ and $\frac{d\theta^{\mathrm{TL}}_{(\bar{\mu})}}{d\tau}$ turn out to be

$$\theta^{\mathrm{TL}}_{(\bar{\mu})} = \pm \frac{1}{2\gamma\sqrt{p_c}}\left\{2\frac{\sin(\bar{\mu}_b b)}{\bar{\mu}_b}\cos(\bar{\mu}_c c) + \left[\frac{\sin(\bar{\mu}_b b)}{\bar{\mu}_b} - \frac{\bar{\mu}_b}{\sin(\bar{\mu}_b b)}\gamma^2\right]\cos(\bar{\mu}_b b)\right\}, \tag{92}$$

$$\begin{aligned}\frac{d\theta^{\mathrm{TL}}_{(\bar{\mu})}}{d\tau} =& \frac{1}{8p_c}\left\{-3 + \frac{\sin^2(\bar{\mu}_b b)}{\bar{\mu}_b^2}\left[\frac{17}{2\gamma^2} - \frac{8}{\gamma^2}\cos(\bar{\mu}_b b)\cos(\bar{\mu}_c c) - \frac{16}{\gamma^2}\cos(2\bar{\mu}_c c)\right]\right.\\ &\left. - \frac{3\gamma^2}{2}\frac{\bar{\mu}_b^2}{\sin^2(\bar{\mu}_b b)} - \left[\frac{5}{2\gamma^2}\frac{\sin^2(\bar{\mu}_b b)}{\bar{\mu}_b^2} + \frac{\gamma^2}{2}\frac{\bar{\mu}_b^2}{\sin^2(\bar{\mu}_b b)} + 1\right]\cos(2\bar{\mu}_b b)\right\}.\end{aligned} \tag{93}$$

Notice that these expressions should in fact be thought of being in terms of Δ. Furthermore, note that the form of $\theta^{\mathrm{TL}}_{(\bar{\mu})}$ is exactly the same as the $\mathring{\mu}$ case but with $\mathring{\mu}$ replaced by $\bar{\mu}$. The perturbative expansion of these expressions for small Δ become (negative branch for the expansion scalar)

$$\theta^{\mathrm{TL}}_{(\bar{\mu})} \approx -\frac{1}{2\gamma\sqrt{p_c}}\left[3b - \frac{\gamma^2}{b} - \left(\frac{b^3}{p_b} + \frac{bc^2}{p_c} - \frac{b\gamma^2}{3p_b}\right)\Delta\right] + \mathcal{O}\left(\Delta^2\right), \tag{94}$$

$$\frac{d\theta^{\mathrm{TL}}_{(\bar{\mu})}}{d\tau} \approx -\frac{1}{2p_c}\left[1 + \frac{9b^2}{2\gamma^2} + \frac{\gamma^2}{2b^2} - \left[\frac{15b^4}{4\gamma^2 p_b} + \frac{9b^2c^2}{\gamma^2 p_c} + \frac{b^2}{2p_b} + \frac{\gamma^2}{12p_b}\right]\Delta\right] + \mathcal{O}\left(\Delta^2\right). \tag{95}$$

The behavior of the solution to the canonical variables is such that the combination of the effective terms above are not only positive, but also become very large and balance the classical terms and lead to cancellation of focusing of the congruence at $t = 0$. This can be seen from the full nonperturbative behavior of $\theta^{\mathrm{TL}}_{(\bar{\mu})}$ and $\frac{d\theta^{\mathrm{TL}}_{(\bar{\mu})}}{d\tau}$ depicted in Figure 8.

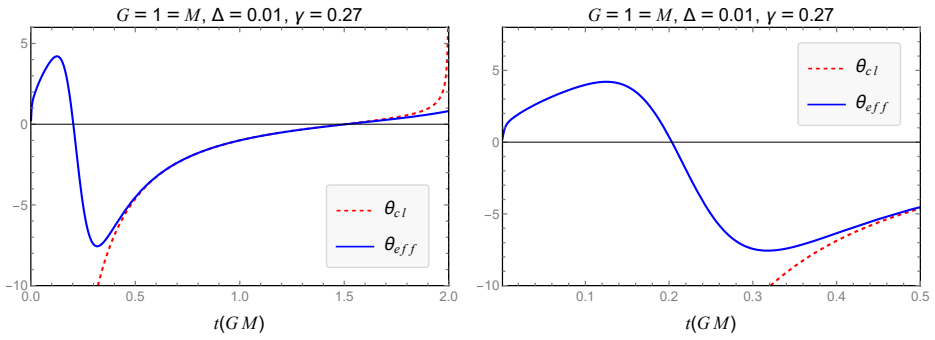

(**a**)

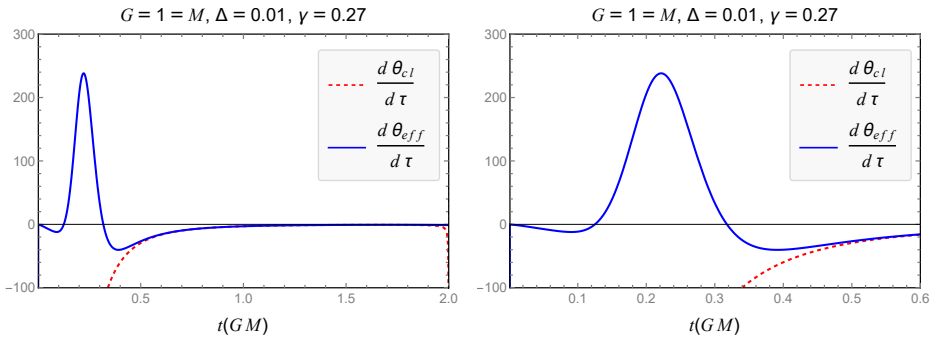

(**b**)

Figure 8. $\theta^{\mathrm{TL}}_{(\bar{\mu})}$ and $\frac{d\theta^{\mathrm{TL}}_{(\bar{\mu})}}{d\tau}$. (**a**) Left: Classical vs timlike θ in the $\bar{\mu}$ scheme as a function of the Schwarzschild time t. The effective expansion $\theta^{\mathrm{TL}}_{(\bar{\mu})}$ goes to zero as $t \to 0$. Right: Close up of the left figure close to $t = 0$. (**b**) Left: Classical vs. timlike $\frac{d\theta}{d\tau}$ in the $\bar{\mu}$ scheme as a function of the Schwarzschild time t. The effective $\frac{d\theta^{\mathrm{TL}}_{(\bar{\mu})}}{d\tau}$ goes to zero as $t \to 0$. Right: Close up of the left figure close to $t = 0$.

In the same way, we can compute the null expansion scalar and Raychaudhuri equation using Equations (44) and (46) and the equations of motion of this scheme. Doing so, one obtains

$$\theta^{\mathrm{NL}}_{(\bar{\mu})} = \pm \frac{2}{\gamma\sqrt{p_c}} \frac{\sin(\bar{\mu}_b b)}{\bar{\mu}_b} \cos(\bar{\mu}_c c), \tag{96}$$

$$\frac{d\theta^{\mathrm{NL}}_{(\bar{\mu})}}{d\lambda} = \frac{2}{\gamma^2 p_c} \left\{ \frac{\sin^2(\bar{\mu}_b b)}{\bar{\mu}_b^2} \left[\frac{3}{2} - \frac{3}{2}\cos(2\bar{\mu}_c c) - \cos(\bar{\mu}_b b)\cos(\bar{\mu}_c c) \right] \right\},$$

with perturbative forms (negative branch for the expansion scalar)

$$\theta^{\mathrm{NL}}_{(\bar{\mu})} \approx -\frac{1}{\gamma\sqrt{p_c}} \left[2b - \left(\frac{b^3}{3p_b} + \frac{bc^2}{p_c} \right) \Delta \right] + \mathcal{O}\left(\Delta^2\right), \tag{97}$$

$$\frac{d\theta^{\mathrm{NL}}_{(\bar{\mu})}}{d\lambda} \approx \frac{1}{\gamma^2 p_c} \left[-2b^2 + \left(\frac{5b^4}{3p_b} + 7b^2c^2 \right) \Delta \right] + \mathcal{O}\left(\Delta^2\right). \tag{98}$$

One can make similar observation about these expressions by noting that the effective terms are positive and take over close to $t = 0$. These observations are confirmed by plotting the full nonperturbative expressions in Figure 9, where it is seen that nowhere inside the black hole does either $\theta^{\mathrm{NL}}_{(\bar{\mu})}$ or $\frac{d\theta^{\mathrm{NL}}_{(\bar{\mu})}}{d\lambda}$ blow up.

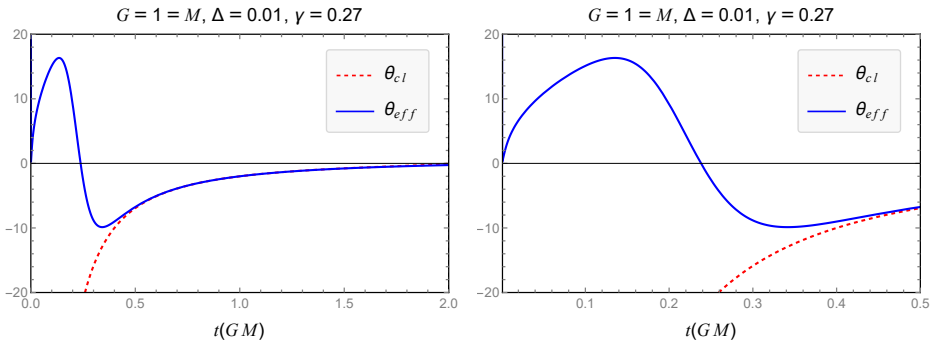

(**a**)

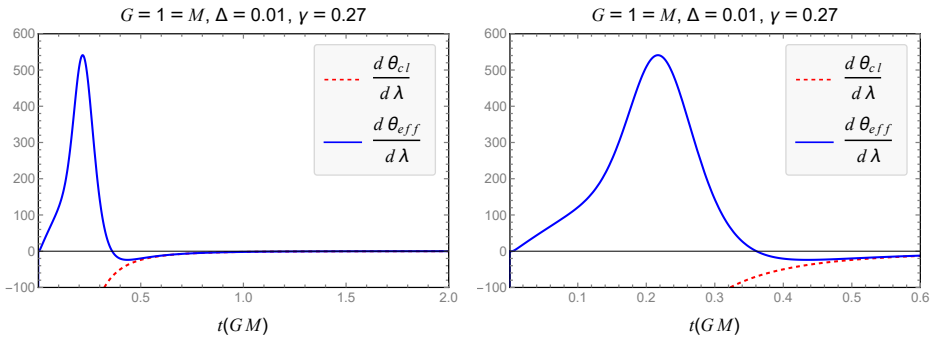

(**b**)

Figure 9. $\theta^{\rm NL}_{(\bar{\mu})}$ and $\frac{d\theta^{\rm NL}_{(\bar{\mu})}}{d\lambda}$. (**a**) Left: Classical vs. null θ in the $\bar{\mu}$ scheme as a function of the Schwarzschild time t. The effective expansion $\theta^{\rm NL}_{(\bar{\mu})}$ goes to zero as $t \to 0$. Right: Close up of the left figure close to $t = 0$. (**b**) Left: Classical vs. null $\frac{d\theta}{d\lambda}$ in the $\bar{\mu}$ scheme as a function of the Schwarzschild time t. The effective $\frac{d\theta^{\rm NL}_{(\bar{\mu})}}{d\lambda}$ goes to zero as $t \to 0$. Right: Close up of the left figure close to $t = 0$.

The Kretschmann scalar in this case has a similar behavior to the previous case. However, while it does not diverge, it becomes quite large at $t \to 0$. By looking at its profile in Figure 10, we see that not only it does not diverge anywhere in the interior, but also it becomes zero as $t \to 0$. Since the full expression for K in this case is also very large, let us first check the perturbative expression up to Δ,

$$\begin{aligned} K = \frac{1}{p_c^2}\Bigg[12 + \frac{12b^4}{\gamma^4} + \frac{24b^2}{\gamma^2} \\ - \Delta\left(\frac{b^6}{\gamma^4 p_b} + \frac{76b^4c^2}{\gamma^4 p_c} + \frac{7b^4}{\gamma^2 p_b} + \frac{88b^2c^2}{\gamma^2 p_c} + \frac{7b^2}{p_b} + \frac{12c^2}{p_c} + \frac{\gamma^2}{p_b}\right) \\ + \mathcal{O}\left(\Delta^2\right). \end{aligned} \tag{99}$$

The same pattern emerges here too similar to the previous case where the correction terms are all negative, given the behavior of the solutions to the equations of motion, particularly of p_b, p_c. These effective terms will counter the classical terms and become large close to the region used to be the singularity, thus stopping K from diverging. However, in this model, K does not vanish at $t = 0$. Based on the value we chose for Δ, we obtain $K \approx 3 \times 10^{36}$ for $t = 0$. This is seen from the full numerical nonperturbative behavior of K as a function of the Schwarzschild time t in Figure 10.

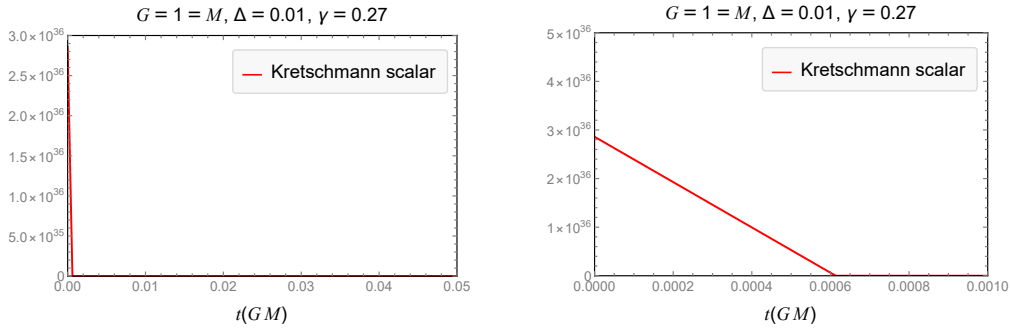

(**a**) (**b**)

Figure 10. K in the $\bar{\mu}$ case. (**a**) The Kretschmann scalar K for the $\bar{\mu}$ case as a function of the Schwarzschild time t. (**b**) Close up of K close to $t = 0$. It is seen that K remains finite everywhere in the interior although it does not vanishes for $t = 0$.

4.1.3. $\bar{\mu}'$ Scheme

Here $\bar{\mu}'_b$, $\bar{\mu}'_c$ have the following dependence on the triad components,

$$\bar{\mu}'_b = \sqrt{\frac{\Delta}{p_c}}, \tag{100}$$

$$\bar{\mu}'_c = \frac{\sqrt{p_c \Delta}}{p_b}, \tag{101}$$

and the equations of motion in this case are

$$\frac{db}{dT} = -\frac{1}{2}\gamma^2 \frac{\bar{\mu}'_b}{\sin(\bar{\mu}'_b b)} - \frac{1}{2}\frac{\sin(\bar{\mu}'_b b)}{\bar{\mu}'_b} - \frac{p_c}{p_b}\left[\frac{\sin(\bar{\mu}'_c c)}{\bar{\mu}'_c} + c\cos(\bar{\mu}'_c c)\right], \tag{102}$$

$$\frac{dp_b}{dT} = \frac{1}{2} p_b \cos(\bar{\mu}'_b b)\left[1 - \gamma^2 \frac{\bar{\mu}'^2_b}{\sin^2(\bar{\mu}'_b b)}\right], \tag{103}$$

$$\frac{dc}{dT} = \frac{p_b}{2p_c}\left[\gamma^2 \frac{\bar{\mu}'_b}{\sin(\bar{\mu}'_b b)}\left[1 - \frac{\bar{\mu}'_b}{\sin(\bar{\mu}'_b b)} b\cos(\bar{\mu}'_b b)\right] - \frac{\sin(\bar{\mu}'_b b)}{\bar{\mu}'_b}\right] + \frac{b p_b \cos(\bar{\mu}'_b b)}{2p_c} - \frac{\sin(\bar{\mu}'_c c)}{\bar{\mu}'_c} - c\cos(\bar{\mu}'_c c), \tag{104}$$

$$\frac{dp_c}{dT} = 2p_c \cos(\bar{\mu}'_c c). \tag{105}$$

These equations can also be solved numerically as before. By demanding the solutions match the classical ones at the horizon $t \to 2GM$, we obtain the behavior of the canonical variables as depicted in Figure 11.

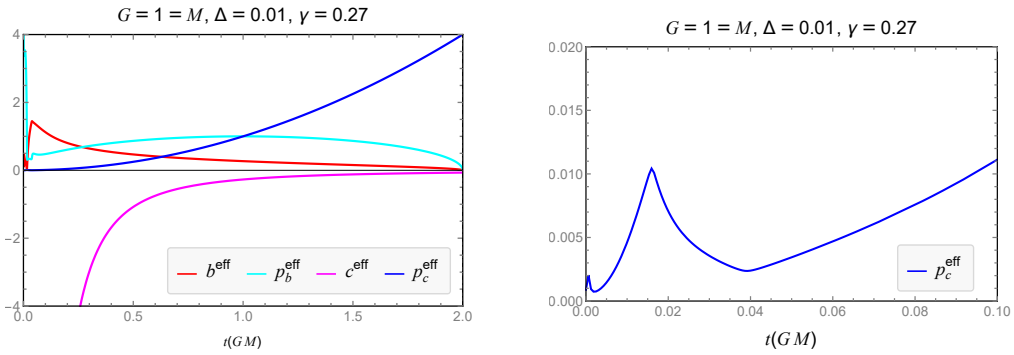

(**a**) (**b**)

Figure 11. Solutions of the EoM of the $\bar{\mu}$ case. (**a**) Solutions to the equations of motion in the $\bar{\mu}'$ case as a function of the Schwarzschild time t. (**b**) Close up of the left figure close to $t = 0$. Although p_c behaves rather erratically close to $t = 0$, it never vanishes in this case either.

With the help of these equations and their solutions together with Eqautions (43) and (45), we can obtain the following expressions for the expansion scalar and the Raychaudhuri equation

$$\theta^{\mathrm{TL}}_{(\bar{\mu}')} = \pm \frac{1}{2\gamma\sqrt{p_c}} \left\{ 2\frac{\sin(\bar{\mu}'_b b)}{\bar{\mu}'_b}\cos(\bar{\mu}'_c c) + \left[\frac{\sin(\bar{\mu}'_b b)}{\bar{\mu}'_b} - \gamma^2 \frac{\bar{\mu}'_b}{\sin(\bar{\mu}'_b b)}\right]\cos(\bar{\mu}'_b b)\right\}, \tag{106}$$

$$\begin{aligned}
\frac{d\theta^{\mathrm{TL}}_{(\bar{\mu}')}}{d\tau} =& \frac{1}{8p_c} + \frac{\bar{\mu}'_b \cos(\bar{\mu}'_b b)\sin(\bar{\mu}'_c c)}{2}\left(\frac{b}{p_c} - \frac{c}{2p}\right) - \frac{1}{4p_c}\cos(2\bar{\mu}'_b b) + \frac{\cos(\bar{\mu}'_b b)\cos(\bar{\mu}'_c c)}{2p_c} \\
&+ \frac{c}{2p_b\gamma^2}\frac{\sin(\bar{\mu}'_b b)}{\bar{\mu}'_b}\left[-\frac{\cos(\bar{\mu}'_c c)}{2}\left[1-\cos(2\bar{\mu}'_b b)\right] + \cos^2(\bar{\mu}'_b b)\cos(\bar{\mu}'_c c)\right. \\
&\left. +2\cos(\bar{\mu}'_b b)\cos^2(\bar{\mu}'_c c) - \frac{\cos(\bar{\mu}'_b b)}{c}\frac{\sin(2\bar{\mu}'_c c)}{2\bar{\mu}'_c}\right] \\
&+ \frac{b}{2\gamma^2 p_c}\frac{\sin(\bar{\mu}'_b b)}{\bar{\mu}'_b}\left[\frac{\cos(\bar{\mu}'_c c)}{2}\left[1-\cos(2\bar{\mu}'_b b)\right] - \cos^2(\bar{\mu}'_b b)\cos(\bar{\mu}'_c c)\right. \\
&\left. -2\cos(\bar{\mu}'_b b)\cos^2(\bar{\mu}'_c c) - \frac{\cos(\bar{\mu}'_b b)}{b}\frac{\sin(2\bar{\mu}'_c c)}{2\bar{\mu}'_c}\right] \\
&+ \frac{b}{4\gamma^2 p_b}\frac{\sin(\bar{\mu}'_c c)}{\bar{\mu}'_c}\left[-\cos(\bar{\mu}'_b b)\left[1-\cos(2\bar{\mu}'_b b)\right]\right] \\
&+ \frac{cp_c}{4\gamma^2 p_b^2}\frac{\sin(\bar{\mu}'_c c)}{\bar{\mu}'_c}\left[\cos(\bar{\mu}'_b b)\left[1-\cos(2\bar{\mu}'_b b)\right]\right] \\
&+ \frac{1}{2\gamma^2 p_c}\frac{\sin^2(\bar{\mu}'_b b)}{\bar{\mu}'^2_b}\left[1 - \frac{3\cos(2\bar{\mu}'_b b)}{2} - \cos(\bar{\mu}'_b b)\cos(\bar{\mu}'_c c)\right] \\
&+ \frac{1}{2\gamma^2 p_b}\frac{\sin(\bar{\mu}'_b b)}{\bar{\mu}'_b}\frac{\sin(\bar{\mu}'_c c)}{\bar{\mu}'_c}\left[1 - \cos^2(\bar{\mu}'_b b) - \cos(2\bar{\mu}'_b b) - \gamma^2\bar{\mu}'_b\bar{\mu}'_c\frac{p_b}{p_c}\right] \\
&+ \frac{1}{2}\frac{\bar{\mu}'_b}{\sin(\bar{\mu}'_b b)}\left[\left(\frac{c}{p_b} - \frac{b}{p_c}\right)\cos(\bar{\mu}'_c c) - \frac{1}{p_b}\frac{\sin(\bar{\mu}'_c c)}{\bar{\mu}'_c} - \frac{\gamma^2}{2p_c}\frac{\bar{\mu}'_b}{\sin(\bar{\mu}'_b b)}\right].
\end{aligned} \tag{107}$$

Here also the form of $\theta^{\rm TL}_{(\bar{\mu}')}$ is exactly the same as the $\mathring{\mu}$ and $\bar{\mu}$ cases but with $\mathring{\mu}$ and $\bar{\mu}$ replaced by $\bar{\mu}'$. The perturbative expressions corresponding to these results for $\Delta \to 0$ are

$$\theta^{\rm TL}_{(\bar{\mu}')} \approx -\frac{1}{2\gamma\sqrt{p_c}}\left[3b - \frac{\gamma^2}{b} - \left(\frac{b^3}{p_c^2} + \frac{bc^2p_c}{p_b^2} - \frac{b\gamma^2}{3p_c^2}\right)\Delta\right] + \mathcal{O}\left(\Delta^2\right), \tag{108}$$

$$\begin{aligned}\frac{d\theta^{\rm TL}_{(\bar{\mu}')}}{d\tau} \approx &-\frac{1}{2p_c}\left\{\frac{9b^2}{2\gamma^2} + \frac{\gamma^2}{2b^2} + \right.\\ &\left. +\Delta\left[\frac{\gamma^2}{6p_c} - \frac{b^2}{3p_c} - \frac{11b^4}{2\gamma^2 p_c} + \frac{c^2p_c}{p_b^2}\left(1 - \frac{6b^2}{\gamma^2}\right) + \frac{c^3p_c^2}{p_b^3}\left(\frac{b}{\gamma^2} + \frac{1}{3b}\right)\right]\right\}\\ &+\mathcal{O}\left(\Delta^2\right).\end{aligned} \tag{109}$$

It is not very clear from $\frac{d\theta^{\rm TL}_{(\bar{\mu}')}}{d\tau}$ that whether the effective terms are overall positive or negative since they contain a mixture of positive and negative terms. However, due to the behavior of the solutions of the equations of motion, indeed their overall sign close to $t \to 0$ is positive and they almost cancel out the classical focusing terms. In fact $\theta^{\rm TL}_{(\bar{\mu}')}$ at $t \to 0$ is a small positive number (in the figure its value is 13.6) while $\frac{d\theta^{\rm TL}_{(\bar{\mu}')}}{d\tau} \to 0$ for $t \to 0$. These can be better seen in Figure 12, which depicts the full nonperturbative behavior of these terms.

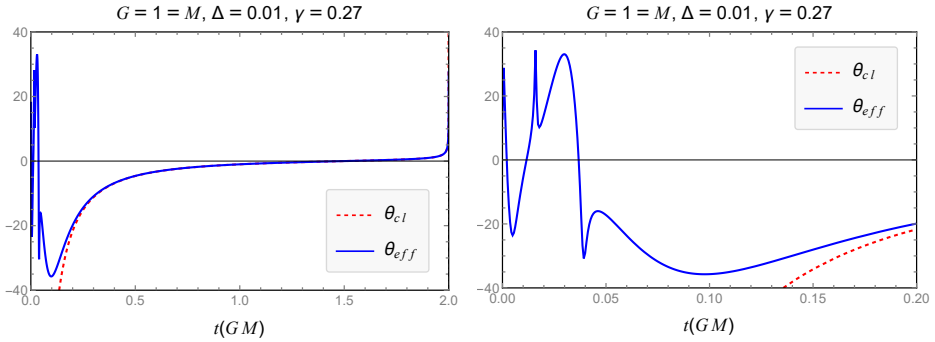

(**a**)

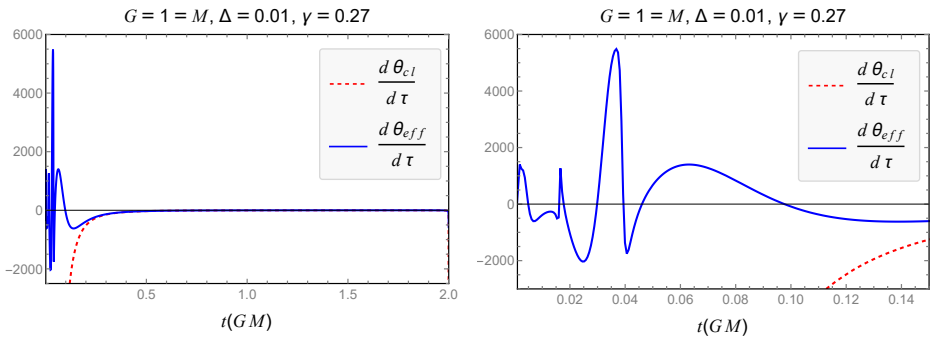

(**b**)

Figure 12. $\theta^{\rm TL}_{(\bar{\mu}')}$ and $\frac{d\theta^{\rm TL}_{(\bar{\mu}')}}{d\tau}$. (**a**) Left: Classical vs. timlike θ in the $\bar{\mu}'$ scheme as a function of the Schwarzschild time t. The effective $\theta^{\rm TL}_{(\bar{\mu}')}$ goes to zero as $t \to 0$. Right: Close up of the left figure close to $t = 0$. (**b**) Left: Classical vs. timlike $\frac{d\theta}{d\tau}$ in the $\bar{\mu}'$ scheme as a function of the Schwarzschild time t. The effective $\frac{d\theta^{\rm TL}_{(\bar{\mu}')}}{d\tau}$ goes to zero as $t \to 0$. Right: Close up of the left figure close to $t = 0$.

By replacing our lapse Equation (67) and differential equations of motion for this case into Equations (44) and (46), we obtain the null expansion scalar and the Raychaudhuri equation as follows

$$\theta^{\rm NL}_{(\bar{\mu}')} = \pm\frac{2}{\gamma\sqrt{p_c}}\frac{\sin(\bar{\mu}'_b b)}{\bar{\mu}'_b}\cos(\bar{\mu}'_c c) \tag{110}$$

$$\begin{aligned}\frac{d\theta^{\rm NL}_{(\bar{\mu}')}}{d\lambda} =& \frac{\bar{\mu}'_c\cos(\bar{\mu}'_b b)\sin(\bar{\mu}'_c c)}{p_c^2}(bp_b - cp_c)\\ &+\frac{2}{\gamma^2}\frac{\sin(2\bar{\mu}'_b b)}{2\bar{\mu}'_b}\cos^2(\bar{\mu}'_c c)\left[\frac{c}{p_b}-\frac{b}{p_c}\right]\\ &+\frac{1}{2}\frac{cp_c\cos(\bar{\mu}'_b b)}{\gamma^2 p_b^2}\frac{\sin(\bar{\mu}'_c c)}{\bar{\mu}'_c}\left[1-\cos(\bar{\mu}'_b b)\right]\\ &+\frac{1}{2\gamma^2 p_b}\frac{\sin(\bar{\mu}'_b b)}{\bar{\mu}'_b}\frac{\sin(\bar{\mu}'_c c)}{\bar{\mu}'_c}\left[1-\cos(\bar{\mu}'_b b)\right]\\ &+\frac{1}{\gamma^2 p_c}\frac{\sin^2(\bar{\mu}'_b b)}{\bar{\mu}'^2_b}\left[1-\cos(\bar{\mu}'_c c)\left(1+2\cos(\bar{\mu}'_b b)-2\cos(\bar{\mu}'_c c)\right)\right]\\ &-\frac{\sin(2\bar{\mu}'_b b)}{2\bar{\mu}'_b\gamma^2 p_b}\left[b\bar{\mu}'_b\sin(\bar{\mu}'_b b)\frac{\sin(\bar{\mu}'_c c)}{\bar{\mu}'_c}+\frac{\sin(2\bar{\mu}'_c c)}{\bar{\mu}'_c}\right]\\ &-\frac{\sin(\bar{\mu}'_b b)\sin(\bar{\mu}'_c c)}{p_c}.\end{aligned} \tag{111}$$

which are a bit simpler expressions compared to the timelike case. These have perturbative forms (negative branch for the expansion scalar)

$$\theta^{\rm NL}_{(\bar{\mu}')} \approx -\frac{1}{\gamma\sqrt{p_c}}\left[2b-\left(\frac{b^3}{3p_c}+\frac{bc^2p_c}{p_b^2}\right)\Delta\right]+\mathcal{O}\left(\Delta^2\right), \tag{112}$$

$$\frac{d\theta^{\rm NL}_{(\bar{\mu}')}}{d\lambda} \approx -\frac{2b^2}{\gamma^2 p_c}+\left(\frac{7b^4}{3\gamma^2p_c^2}+\frac{4b^2c^2}{\gamma^2p_b^2}-\frac{2bc^3p_c}{3\gamma^2p_b^3}-\frac{c^2}{p_b^2}\right)\Delta+\mathcal{O}\left(\Delta^2\right). \tag{113}$$

For $\theta^{\rm NL}_{(\bar{\mu}')}$ in this approximation, it is clear that the effective terms are positive, and in fact they become significant near $t=0$. In case of $\frac{d\theta^{\rm NL}_{(\bar{\mu}')}}{d\lambda}$, it is not quite clear whether the combination of the effective terms is positive or negative, but due to the behavior of the solutions to the equations of motion, these turn out to be positive close to $t=0$ and become quite significant there. The full nonperturbative behavior is plotted in Figure 13 and it is seen that both $\theta^{\rm NL}_{(\bar{\mu}')}$ and $\frac{d\theta^{\rm NL}_{(\bar{\mu}')}}{d\lambda}$ go to zero as $t\to 0$. The Kretschmann scalar always in this remains finite just as the two previous cases. Due to the erratic behavior of the solutions to the equations of motion, K starts oscillating close to $t=0$, but nevertheless it always remains finite. Let us first check the perturbative expression of K up to Δ,

$$\begin{aligned}K =& \frac{1}{p_c^2}\left[12+\frac{24b^2}{\gamma^2}+\frac{12b^4}{\gamma^4}\right.\\ &-\Delta\left(\frac{2b^6}{\gamma^4p_c}+\frac{52b^4p_cc^2}{\gamma^4p_b^2}+\frac{26b^4}{3\gamma^2p_c}+\frac{56p_cb^2c^2}{\gamma^2p_b^2}+\frac{26b^2}{3p_c}\right.\\ &\left.\left.+\frac{4p_cc^3}{3bp_b^3}+\frac{4p_cc^2}{p_b^2}+\frac{2\gamma^2}{p_c}-\frac{4b^3p_c^2c^3}{\gamma^4p_b^3}-\frac{8p_cbc^3}{3\gamma^2p_b^3}\right)\right]\\ &+\mathcal{O}\left(\Delta^2\right).\end{aligned} \tag{114}$$

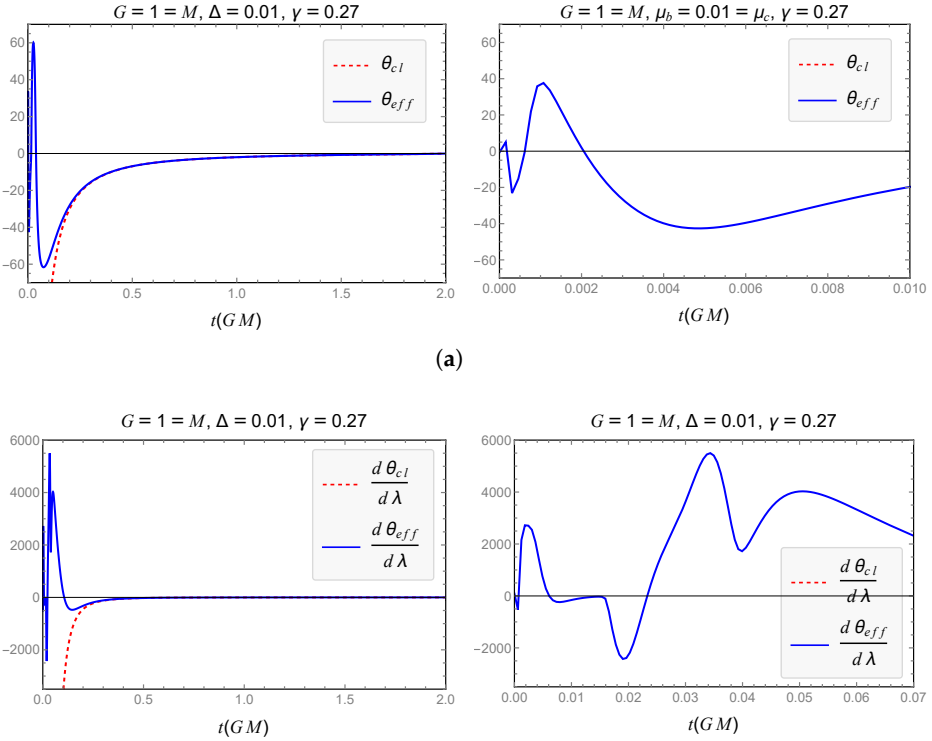

Figure 13. $\theta^{\mathrm{NL}}_{(\bar{\mu}')}$ and $\frac{d\theta^{\mathrm{NL}}_{(\bar{\mu}')}}{d\lambda}$. (**a**) Left: Classical vs. null θ in the $\bar{\mu}'$ scheme as a function of the Schwarzschild time t. The effective expansion $\theta^{\mathrm{NL}}_{(\bar{\mu}')}$ goes to zero as $t \to 0$. Right: Close up of the left figure close to $t = 0$. (**b**) Left: Classical vs. null $\frac{d\theta}{d\lambda}$ in the $\bar{\mu}'$ scheme as a function of the Schwarzschild time t. The effective $\frac{d\theta^{\mathrm{NL}}_{(\bar{\mu}')}}{d\lambda}$ goes to zero as $t \to 0$. Right: Close up of the left figure close to $t = 0$.

The correction terms in this case are not all negative, although most of them are. It turns out that the full K behaves in the desired way. It stays finite everywhere and goes to zero for $t = 0$. This can be seen from Figure 14.

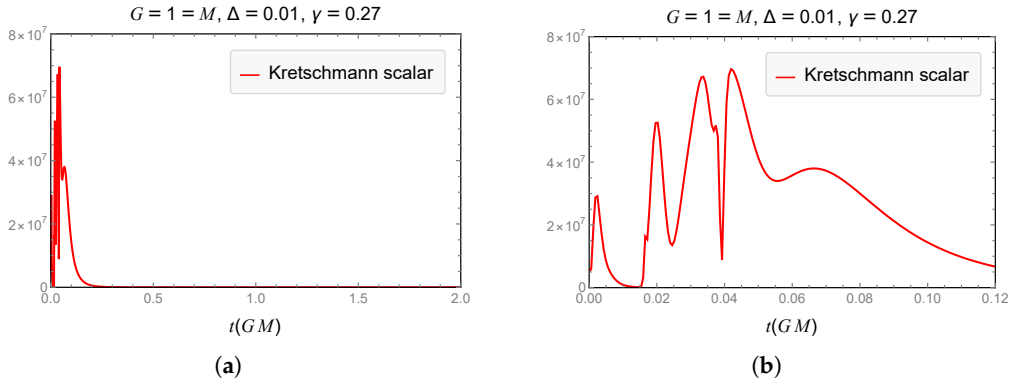

(**a**) (**b**)

Figure 14. K in the $\bar{\mu}'$ case. (**a**) The Kretschmann scalar K for the $\bar{\mu}'$ case as a function of the Schwarzschild time t. (**b**) Close up of K close to $t = 0$. It is seen that K remains finite everywhere in the interior and vanishes for $t = 0$.

4.2. Generalized Uncertainty Principle

In the case of the generalized uncertainty principle (GUP), the standard Heisenberg algebra of the system is effectively modified. Inspired by the above, and the fact that a corrected quantum algebra also implies suitable modifications of the corresponding Poisson

algebra, one can assume that the fundamental Poisson brackets between the canonical variables also get modified as

$$\{b, p_b\} = G\gamma F_1(b, c, p_b, p_c, \beta_b, \beta_c), \tag{115}$$
$$\{c, p_c\} = 2G\gamma F_2(b, c, p_b, p_c, \beta_b, \beta_c), \tag{116}$$

where the modifications are encoded entirely in F_1 and F_2, and hence the non-deformed classical limit is obtained by setting $F_1 = 1 = F_2$. Here, β_i refer to the parameters by which the algebra is modified. Such modification will result in the effective equations of motion

$$\frac{db}{dT} = \{b, H\} = -\frac{1}{2}\left(b + \frac{\gamma^2}{b}\right)F_1, \tag{117}$$
$$\frac{dp_b}{dT} = \{p_b, H\} = \frac{p_b}{2}\left(1 - \frac{\gamma^2}{b^2}\right)F_1, \tag{118}$$
$$\frac{dc}{dT} = \{c, H\} = -2cF_2, \tag{119}$$
$$\frac{dp_c}{dT} = \{p_c, H\} = 2p_cF_2. \tag{120}$$

which should also be supplemented by weakly vanishing of the Hamiltonian constraint Equation (48). Notice that in this approach the Hamiltonian does not get modified and the effective modifications to the equations of motion come from the modifications to the Poisson algebra.

The above equations of motion Equations (117)–(120) can now be substituted into the timelike expansion Equation (43) and Raychaudhuri Equation (45) to yield (with $N = \frac{\gamma\sqrt{p_c}}{b}$ as before):

$$\theta^{(\mathrm{TL})}_{\mathrm{GUP}} = \pm\frac{1}{2\gamma\sqrt{p_c}}\left(bF_1 - \frac{\gamma^2F_1}{b} + 2bF_2\right), \tag{121}$$

and

$$\frac{d\theta^{(\mathrm{TL})}_{\mathrm{GUP}}}{d\tau} = \frac{1}{2\gamma^2p_c}\left[\left(b^2 - \gamma^2\right)\dot{F}_1 + 2b^2\dot{F}_2 - F_1^2\left(\frac{b^2}{2} + \frac{\gamma^4}{2b^2} + \gamma^2\right) - 2b^2F_1F_2 - 2b^2F_2^2\right] \tag{122}$$

in terms of the canonical variables. For the null case, using Equations (44) and (46) we get

$$\theta^{(\mathrm{NL})}_{\mathrm{GUP}} = \frac{2bF_2}{\gamma\sqrt{p_c}}, \tag{123}$$
$$\frac{d\theta^{(\mathrm{NL})}_{\mathrm{GUP}}}{d\lambda} = \frac{2b^2}{\gamma^2p_c}\left(\dot{F}_2 - F_1F_2\right). \tag{124}$$

As can be seen from Equations (115) and (116), the modifications to the Poisson algebra is controlled by functions F_1 and F_2. A generic class of modifications, containing terms up to second order in canonical variables and with no cross terms, can be written as

$$F_i = 1 + \alpha_b^{(i)}b + \alpha_c^{(i)}c + \beta_b^{(i)}b^2 + \beta_c^{(i)}c^2 + \alpha_b'^{(i)}p_b + \alpha_c'^{(i)}p_c + \beta_b'^{(i)}p_b^2 + \beta_c'^{(i)}p_c^2, \tag{125}$$

where α_l, β_l, α_l', β_l' parameters (with $l = b, c$) encode the quantum gravity effects associated to the noncommutativity of the model, and $i = 1, 2$. We will consider the four most common cases appearing in the literature,

$$\text{Model 1}: \quad F_1 = 1 + \beta_b b^2, \quad F_2 = 1 + \beta_c c^2, \tag{126}$$
$$\text{Model 2}: \quad F_1 = 1 + \alpha_b' p_b, \quad F_2 = 1 + \alpha_c' p_c, \tag{127}$$
$$\text{Model 3}: \quad F_1 = 1 + \alpha_b b, \quad F_2 = 1 + \alpha_c c, \tag{128}$$
$$\text{Model 4}: \quad F_1 = 1 + \beta_b' p_b^2, \quad F_2 = 1 + \beta_c' p_c^2. \tag{129}$$

In each model, we can consider the parameters α_l, β_l, α'_l, β'_l to be positive, negative or zero. It turns out that only in configuration-dependent cases models 1 and 3 and just for certain signs of α_l, β_l, α'_l, β'_l will both θ and the Raychaudhuri equation remain finite everywhere in the interior. In fact, finding the solutions to the equations of motion Equations (117)–(120) by using either of the momentum-dependent case Equation (127) or (129) and replacing the solutions into any of Equations (121)–(124), one can never obtain a finite value for them as $t \to 0$ for any value of α'_b, α'_c, β'_b, β'_c. This means that the momentum-dependent cases are not viable for modeling GUP if we demand the singularity of the black hole model we are using is resolved. On the other hand configuration-dependent cases do in fact allow for such a possibility. This is summarized in Table 1.

Table 1. Comparison of GUP models with regard to the possibility of singularity resolution.

Model	Dependence of GUP Modifications on	Expansion and RE Finite for
1	Configuration	$\beta_b < 0$ and $\beta_c < 0$
2	Momenta	No values of α'_b and α'_c
3	Configuration	$\alpha_b < 0$ and $\alpha_c > 0$
4	Momenta	No values of β'_b and β'_c

Let us first consider model 1. The solution to the equations of motion in this model are plotted in Figure 15. From this figure we see that none of the variables diverge or vanish in the interior, and everywhere in the interior $b, p_b, p_c > 0$ while $c < 0$. For the chosen values of β_b, β_c, for $t \to 0$ we obtain $b \approx 4$ and $c \approx -4$.

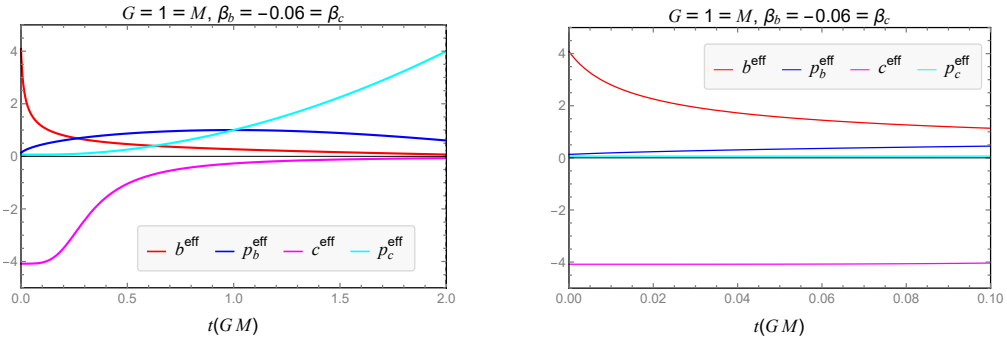

(**a**) (**b**)

Figure 15. Solutions of the EoM of GUP model 1. (**a**) Solutions to the effective equations of motion for model 1 as a function of the Schwarzschild time t. (**b**) Close up of the left figure close to $t = 0$. Note that none of the variables diverge or vanish in the interior, and everywhere in the interior $b, p_b, p_c > 0$ while $c < 0$.

For this model we obtain the expressions for the timelike case

$$\theta^{(\mathrm{TL})}_{\mathrm{GUP}(1)} = \pm \frac{b}{2\gamma\sqrt{p_c}}\left[3 - \frac{\gamma^2}{b^2} + 2\beta_c c^2 + \beta_b\left(b^2 - \gamma^2\right)\right], \tag{130}$$

$$\frac{d\theta^{(\mathrm{TL})}_{\mathrm{GUP}(1)}}{d\tau} = \frac{1}{\gamma^2 p_c}\left[-\frac{9b^2}{4} - \frac{\gamma^4}{4b^2} - \frac{\gamma^2}{2} - \beta_b b^2\left(2b^2 + \gamma^2\right) + \frac{\beta_b^2 b^2}{4}\left(\gamma^4 - 3b^4 - 2\gamma^2 b^2\right) - \beta_c^2 c^2 b^2\left(5c^2 + 7\right) - \beta_b\beta_c b^2 c^2\right] \tag{131}$$

Solving the equations of motion Equations (117)–(120) with Equation (126) and replacing the solutions in the above two expressions, we obtain the behavior of $\theta^{(\mathrm{TL})}_{\mathrm{GUP}}$ and $\frac{d\theta^{(\mathrm{TL})}_{\mathrm{GUP}}}{d\tau}$ as a function of the Schwarzschild time t. It turns out that only the case with both $\beta_b < 0$ and $\beta_c < 0$ will yield expressions that are always finite in the interior. With such choice of β's we can numerically find the expressions for Equations (130) and (131), which are plotted in Figure 16. Interestingly, although the expansion scalar $\theta^{(\mathrm{TL})}_{\mathrm{GUP}}$ dips towrads the negative values and its rate of change $\frac{d\theta^{(\mathrm{TL})}_{\mathrm{GUP}}}{d\tau}$ peaks towards positive values when we get closer to $t \to 0$, at some points quantum effects take over and turn them both back towards zero. The qualitative behavior is similar to the cases in LQG but the difference is that in those cases, the expansion scalar in some regions actually becomes positive and then goes to zero, while here the expansion remain negative (after initially being positive) and it goes to zero from below.

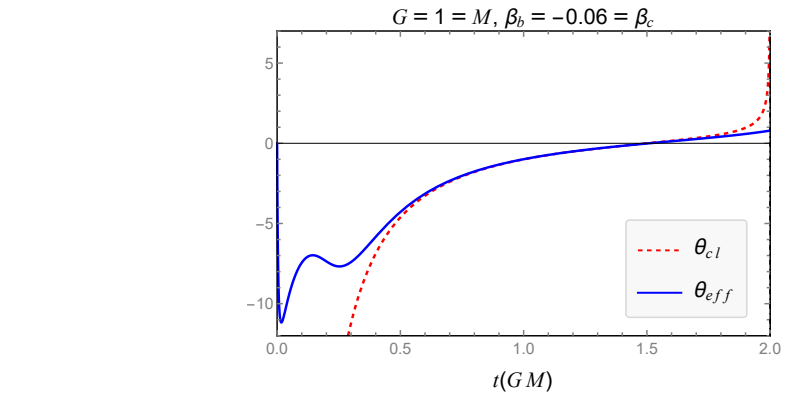

(**a**)

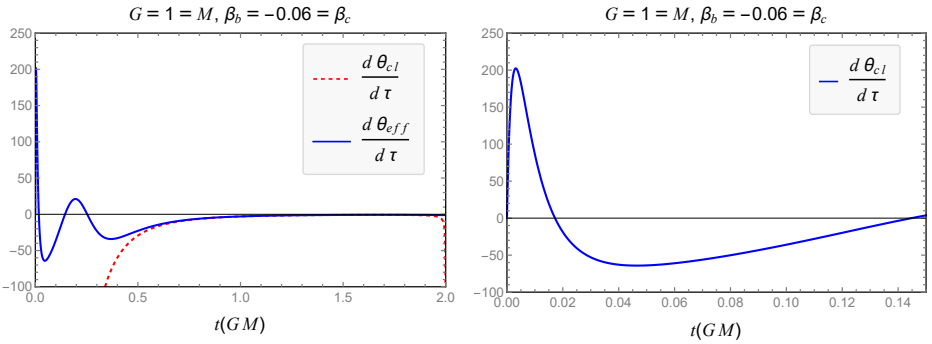

(**b**)

Figure 16. $\theta^{(\mathrm{TL})}_{\mathrm{GUP}(1)}$ and $\frac{d\theta^{(\mathrm{TL})}_{\mathrm{GUP}(1)}}{d\tau}$. (**a**) Classical vs. timelike θ in GUP model 1 as a function of the Schwarzschild time t. (**b**) Left: Classical vs. timelike $\frac{d\theta}{d\tau}$ in GUP model 1 as a function of the Schwarzschild time t. Both the effective effective expansion $\theta^{(\mathrm{TL})}_{\mathrm{GUP}(1)}$ and its rate of change $\frac{d\theta^{(\mathrm{TL})}_{\mathrm{GUP}(1)}}{d\tau}$ go to zero as $t \to 0$. Right: Close up of the left figure close to $t = 0$.

To get an analytical sense of the expressions, we see that for the negative branch of the expansion scalar, Equation (130), the correction terms are all positive (note that $\beta_b < 0$ and $\beta_c < 0$) and it is these terms that overcome the classical negative terms close to $t \to 0$ and turn the curve around. In the same way, in Equation (131) and up to the first order in β's, the correction term $-\beta_b b^2\left(2b^2+\gamma^2\right)$ is positive and has the same effect.

The expressions for the null case for this model become

$$\theta^{(\mathrm{NL})}_{\mathrm{GUP}(1)} = \pm\frac{2b}{\gamma\sqrt{p_c}}\left(1+\beta_c c^2\right) = \pm\frac{2b}{\gamma\sqrt{p_c}}F_2, \tag{132}$$

$$\frac{d\theta^{(\mathrm{NL})}_{\mathrm{GUP}(1)}}{d\lambda} = \frac{1}{\gamma^2 p_c}\left[-2b^2 - 2\beta_b b^4 - 2\beta_c c^2 b^2\left(4\beta_c c^2+5\right) - 2\beta_b\beta_c b^4 c^2\right]. \tag{133}$$

Clearly, with negative β_b and β_c, the correction term in the negative branch of the expansion scalar is positive, and counters the negative classical term. Up to the first order in β, the same is true in the Raychaudhuri equation. In fact the full numerical results once again show that both $\theta^{(\mathrm{NL})}_{\mathrm{GUP}(1)}$ and $\frac{d\theta^{(\mathrm{NL})}_{\mathrm{GUP}(1)}}{d\tau}$ remain finite everywhere inside the black hole as can be seen in Figure 17.

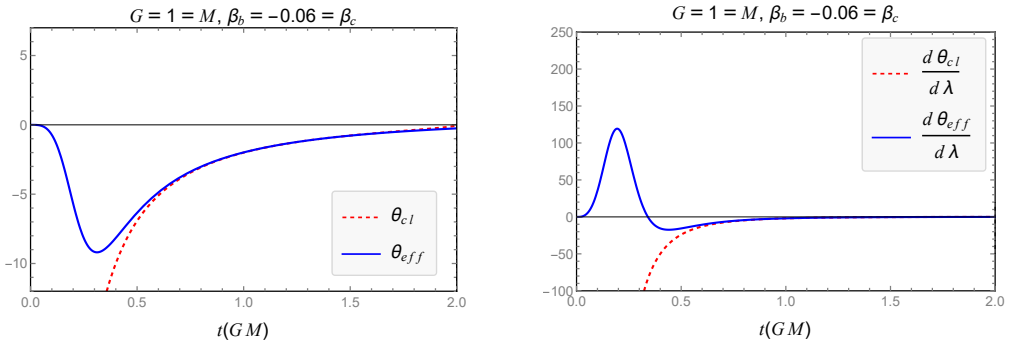

Figure 17. $\theta^{(\mathrm{NL})}_{\mathrm{GUP}(1)}$ and $\frac{d\theta^{(\mathrm{NL})}_{\mathrm{GUP}(1)}}{d\lambda}$. (**a**) Classical vs. null θ in GUP model 1 as a function of the Schwarzschild time t. (**b**) Classical vs. null $\frac{d\theta}{d\tau}$ in GUP model 1 as a function of the Schwarzschild time t. Both the effective expansion $\theta^{(\mathrm{NL})}_{\mathrm{GUP}(1)}$ and its rate of change $\frac{d\theta^{(\mathrm{NL})}_{\mathrm{GUP}(1)}}{d\lambda}$ go to zero as $t \to 0$.

We can also compute the expression for the effective Kretschmann scalar K in this case. This expression is quite large and we do not write it down here. However, the plot of the K in this case is presented in Figure 18. We can clearly see that K remains finite everywhere in the interior particularly for $t \to 0$, although it has a big bump close to this time. This confirms that the quantum effects take over very close to $t = 0$ and keep the curvature finite. In fact $K \to 0$ as $t \to 0$.

Another model for which it is possible to resolve the singularity is model 3 which is the other configuration-dependent case. For the timelike congruence in this model we obtain

$$\theta^{(\mathrm{TL})}_{\mathrm{GUP}(3)} = \pm\frac{1}{2\gamma\sqrt{p_c}}\left[3b - \frac{\gamma^2}{b} + \alpha_b\left(b^2-\gamma^2\right) + 2\alpha_c cb\right], \tag{134}$$

$$\begin{aligned}\frac{d\theta^{(\mathrm{TL})}_{\mathrm{GUP}(3)}}{d\tau} = \frac{1}{2\gamma^2 p_c}\Bigg[&-\frac{9b^2}{2} - \frac{\gamma^4}{2b^2} - \gamma^2 - 10\alpha_c cb^2 \\ &-\alpha_b b\left(\frac{7b^2}{2} + \frac{\gamma^4}{2b^2} + 2\gamma^2\right) - \alpha_b^2 b^4 - \alpha_b^2 b^2\left(\gamma^2+6c^2\right) - 2\alpha_b\alpha_c b^3 c\Bigg].\end{aligned} \tag{135}$$

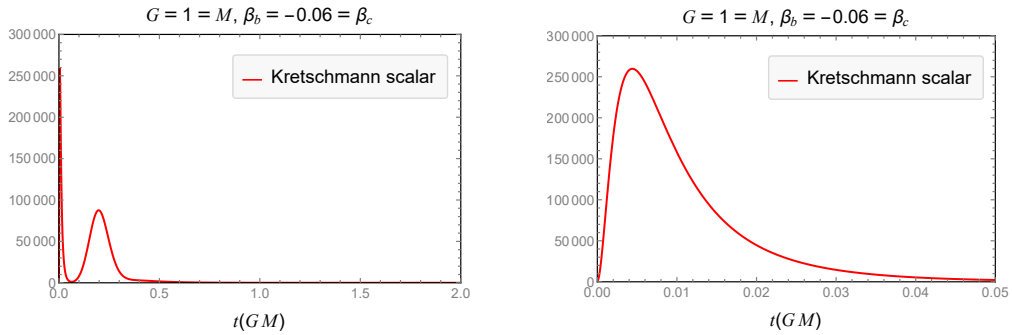

(**a**) (**b**)

Figure 18. K in GUP model 1. (**a**) The Kretschmann scalar K for model 1 as a function of the Schwarzschild time t. (**b**) Close up of K close to $t = 0$. It is seen that K remains finite everywhere in the interior and vanishes for $t = 0$.

It turns out that, as mentioned before, in this model the only case where both the expansion scalar and its rate of change are finite in the interior is when $\alpha_b < 0$ and $\alpha_c > 0$. This can be checked by finding the solutions to the equations of motion for all the cases of the signs of α_b, α_c and checking the behavior of the expansion scalar and Raychaudhuri equation based on them. Having this in mind, we notice that up to the first order in α's, the correction term proportional to α_b in the negative branch of $\theta^{(\mathrm{TL})}_{\mathrm{GUP}(3)}$is positive for $b^2 > \gamma^2$ which is always the case when we get close to $t = 0$. The other correction term $\theta^{(\mathrm{TL})}_{\mathrm{GUP}(3)}$ proportional to α_c is positive for $bc < 0$ which is guaranteed to always hold in the interior based on the solutions to the equations of motions in this model. Up to the same order, the correction term in $\frac{d\theta^{(\mathrm{TL})}_{\mathrm{GUP}(3)}}{d\tau}$ proportional to α_b is clearly always positive. The term proportional to α_c is positive for $c < 0$ which is also guaranteed to hold based on the solutions to the equations of motion. Hence, the first order correction terms contribute to defocusing of the geodesics. This is indeed the case if we also consider the full form of the expressions as can be seen from Figure 19.

We see a difference in this model compared to model 1. Unlike model 1, in model 3 neither $\theta^{(\mathrm{TL})}_{\mathrm{GUP}(3)}$ nor $\frac{d\theta^{(\mathrm{TL})}_{\mathrm{GUP}(3)}}{d\tau}$ become zero at $t = 0$. They both take a finite values (negative and positive, respectively) as can be seen from Figure 19.

The behavior of null congruence for this model results in the following expressions,

$$\theta^{(\mathrm{NL})}_{\mathrm{GUP}(3)} = \pm \frac{2b}{\gamma\sqrt{p_c}}(1 + \alpha_c c) = \pm \frac{2b}{\gamma\sqrt{p_c}} F_2, \tag{136}$$

$$\frac{d\theta^{(\mathrm{NL})}_{\mathrm{GUP}(3)}}{d\lambda} = -\frac{2}{\gamma^2 p_c}\left[b^2 + \alpha_b b^3 + 3\alpha_c b^2 c + \alpha_b \alpha_c b^3 c + 2\alpha_c^2 b^2 c^2\right]. \tag{137}$$

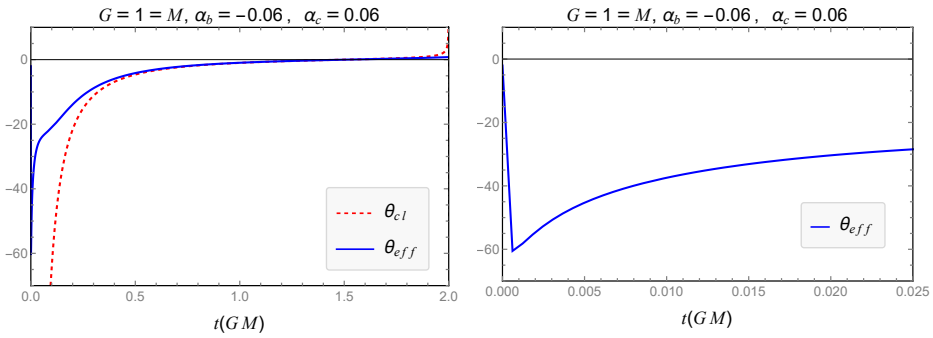

(**a**)

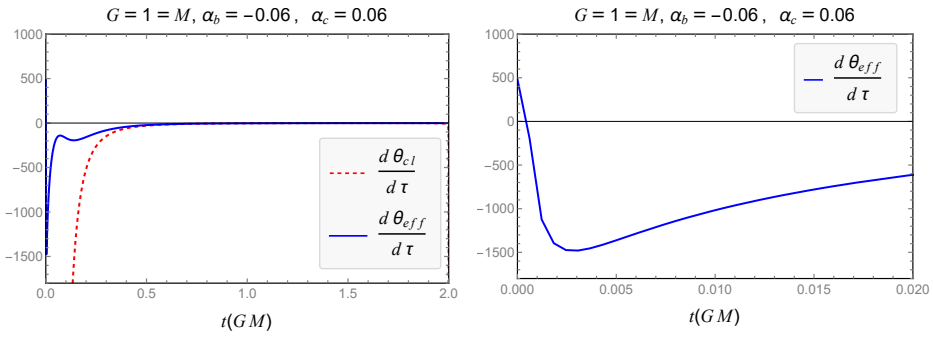

(**b**)

Figure 19. $\theta^{(\mathrm{TL})}_{\mathrm{GUP}(3)}$ and $\frac{d\theta^{(\mathrm{TL})}_{\mathrm{GUP}(3)}}{d\tau}$. Both effective expressions go to finite values as $t \to 0$. (**a**) Left: Classical vs. timelike θ in GUP model 3 as a function of the Schwarzschild time t. Right: Close up of the left figure close to $t = 0$. (**b**) Left: Classical vs. timelike $\frac{d\theta}{d\tau}$ in GUP model 3 as a function of the Schwarzschild time t. Right: Close up of the left figure close to $t = 0$.

Given the behavior of the equations of motion and the signs of α_b, α_c, clearly the correction term up to the first order in α's in the negative branch of $\theta^{(\mathrm{NL})}_{\mathrm{GUP}(3)}$ is positive. The same is true for similar terms in $\frac{d\theta^{(\mathrm{NL})}_{\mathrm{GUP}(3)}}{d\lambda}$. As is expected the full expressions behave in a way that both $\theta^{(\mathrm{NL})}_{\mathrm{GUP}(3)}$ and $\frac{d\theta^{(\mathrm{NL})}_{\mathrm{GUP}(3)}}{d\lambda}$ remain finite everywhere in the interior. This is shown in Figure 20.

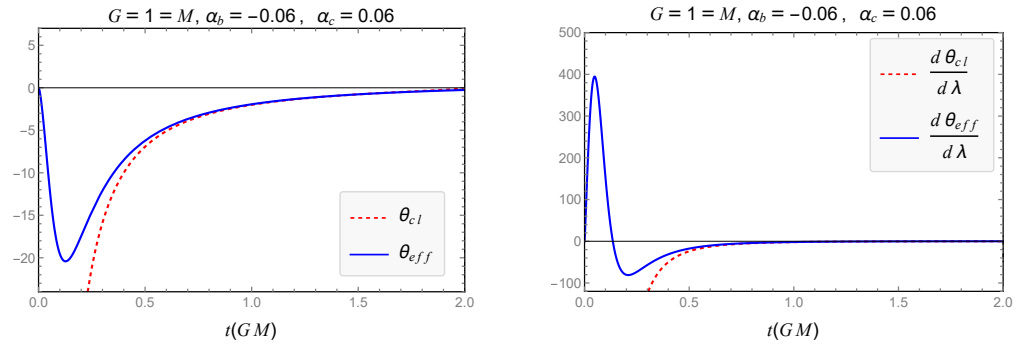

(**a**) (**b**)

Figure 20. $\theta^{(\mathrm{NL})}_{\mathrm{GUP}(3)}$ and $\frac{d\theta^{(\mathrm{NL})}_{\mathrm{GUP}(3)}}{d\lambda}$. Both effective expressions vanish as $t \to 0$. (**a**) Classical vs. null θ in GUP model 3 as a function of the Schwarzschild time t. (**b**) Classical vs. null $\frac{d\theta}{d\tau}$ in GUP model 3 as a function of the Schwarzschild time t.

We see that unlike the timelike case, the null case, $\theta^{(\mathrm{NL})}_{\mathrm{GUP}(3)}$ and $\frac{d\theta^{(\mathrm{NL})}_{\mathrm{GUP}(3)}}{d\lambda}$ actually end up being zero for $t = 0$.

Finally we can derive the Kretschmann scalar K for this model and plot is against t. this is depicted in Figure 21. Once again we see that although there is a big bump in K close to $t = 0$, the quantum effects take over close to that time and turn the curve around such that $k \to 0$ as $t \to 0$. This again confirms that the singularity is resolved due to quantum effects.

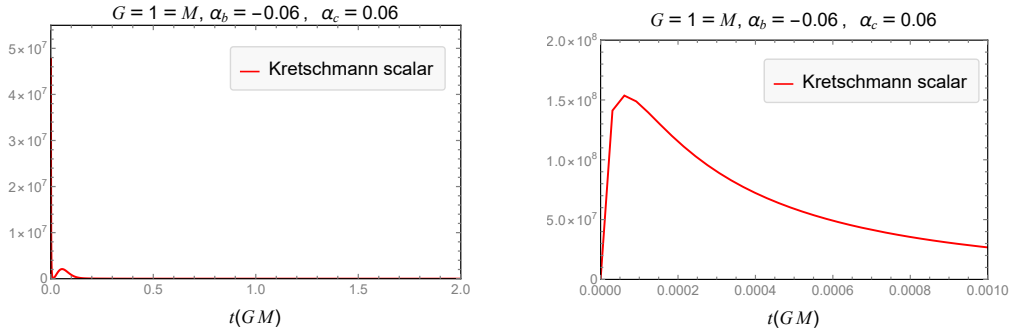

(**a**) (**b**)

Figure 21. K in GUP model 3. (**a**) The Kretschmann scalar K for model 3 as a function of the Schwarzschild time t. (**b**) Close up of K close to $t = 0$. It is seen that K remains finite everywhere in the interior and vanishes for $t = 0$.

5. Discussion

In this work, we have reviewed some of our previous works on probing the interior structure and singularity resolution of the Schwarzschild black hole in LQG and GUP frameworks using expansion scalar and Raychaudhuri equation. We have also presented new results regarding the Kretschmann scalar in both frameworks in addition to new numerical results about GUP models, which leads to eliminating some of them with respect to their ability to resolve the singularity of Schwarzschild interior.

We first present the general form of timelike and null geodesics in the Kantowski-Sachs spacetime which is isometric to the interior of the Schwarzschild black hole. We then derive the timelike and null expansion scalars and their rate of change, i.e., the Raychaudhuri equation for congruences in this metric. All of these quantities depend on the time derivative of metric components or canonical variables, and hence on the solutions to the equations of motion. If the classical Hamiltonian gets modified due to quantum effects, the resulting effective Hamiltonian would yield different equations of motion and hence we will obtain modified expansion scalar and Raychaudhuri equation. This is the route we follow.

We first write the Hamiltonian in terms of the Ashtekar-Barbero connection adapted to this model. Using the equations of motion derived from this Hamiltonian, we compute the expansion scalar θ and its rate of change $\frac{d\theta}{d\tau}$ ($\frac{d\theta}{d\lambda}$ in the null case, with λ the curve parameter) for this classical system. Not surprisingly, both θ and $\frac{d\theta}{d\tau}$ diverse at the center of the black hole where $t \to 0$, where t is the Schwarzschild time in the interior. We then turn into LQG, or more precisely polymer quantization of the Hamiltonian. We use three main schemes of this method, which are different based on the form of the minimum scale introduced in the theory. Using the resulting effective Hamiltonian, we find the new modified solutions to the equations of motion, and find timelike and null θ and $\frac{d\theta}{d\tau}$ ($\frac{d\theta}{d\lambda}$). We show that these effective quantities remain finite everywhere in the interior and never diverge even at $t = 0$. This is shown to be true for all three schemes we studied. We also compute the Kretschmann scalar K analytically and numerically and show that in all three schemes, K remain finite everywhere in the interior. This shows that LQG definitely resolves the singularity.

We then turn to the GUP approach. By modifying the algebra of the canonical variables using GUP parameters α, β we study four most commonly considered model in GUP. Using modified equations of motion, once again we derive timelike and null θ and $\frac{d\theta}{d\tau}$ ($\frac{d\theta}{d\lambda}$) for all the four models. Interestingly, we find that only two of these models, for which the canonical algebra is modified by introducing additional configuration-related terms, have the ability to resolve the singularity. Furthermore not all of the cases of GUP parameters α, β in these two models lead to the singularity resolution. In one of the models (model 1) where the canonical algebra is modified by introducing quadratic terms in configuration variables, the GUP parameters should be both negative to achieve singularity resolution. In the other model (model 3) where the canonical algebra is modified by linear terms in configuration variables, one of the parameters should be negative while the other should be positive, i.e., $\alpha_b < 0$ and $\alpha_c > 0$. Even the inverse of this case, where $\alpha_b > 0$ and $\alpha_c < 0$, does not work. In both of these models with these specific choice of the GUP parameters, not only timelike and null θ and $\frac{d\theta}{d\tau}$ ($\frac{d\theta}{d\lambda}$) remain finite everywhere in the interior, but also the Kretschmann scalar does so.

Hence, we have reaffirmed previous works that claim that all of the LQG models based on a certain polymer quantization resolve the Schwarzschild singularity. Furthermore, we have presented new results excluding certain GUP models by means of their abilities to resolve such a singularity in this Hamiltonian first order framework.

It is interesting to apply this method to works within LQG that use approaches other than the polymer quantization or models which deal with the full spacetime of the Schwrazschild balck hole. One can also apply this method to the full spacetime of the Schwarzschild model but using the GUP framework. These are all interesting works that can be followed in the future.

Author Contributions: Conceptualization, S.R. and S.D.; methodology, S.R. and S.D.; software, S.R. and S.D.; validation, S.R. and S.D.; formal analysis, S.R. and S.D.; investigation, S.R. and S.D.; resources, S.R. and S.D.; data curation, S.R. and S.D.; writing—original draft preparation, S.R. and S.D.; writing—review and editing, S.R. and S.D.; visualization, S.R. and S.D.; supervision, S.R. and S.D.; project administration, S.R. and S.D.; funding acquisition, S.R. and S.D. All authors had contributed equally and have read and agreed to the published version of the manuscript.

Funding: S.D. and S.R. acknowledge the support of the Natural Sciences and Engineering Research Council of Canada (NSERC), [S.D.: funding reference number RGPIN-2019-05404, S.R. funding reference numbers RGPIN-2021-03644 and DGECR-2021-00302].

Institutional Review Board Statement: Not applicable.

Informed Consent Statement: Not applicable.

Data Availability Statement: Not applicable.

Conflicts of Interest: The authors declare no conflict of interest.

Abbreviations

The following abbreviations are used in this manuscript:

LQG	Loop quantum gravity
GUP	Generalized unicertaincty principle
EoM	Equations of motion
GR	General relativity
RE	Raychaudhuri equations

Appendix A. Raychaudhuri Equation

One of the ways to probe the classical and effective structure of spacetime is by investigating the behavior of geodesics. More precisely, how a congruence of timelike or null geodesic evolves over time. This analysis is intimately related to the geodesic deviation

and to the so-called expansion scalar and its rate of change, the Raychaudhuri equation, as we will see below.

Consider a family of curves in a region of spacetime such that through each point in that region, one and only one geodesic passes. This is called a congruence. If every curve in the congruence is timelike/null, then conguence is called timelike/null. In what follows we briefly review both type of these congruences and how they evolve over time.

Appendix A.1. Timelike Congruence

Suppose we have a congruence of timelike geodesics with unit timelike tangent vectors[1] $\{U^a\}$, where

$$g_{ab}U^aU^b = -1, \qquad U^a\nabla_a U^b = 0. \tag{A1}$$

Using these curves, we can decompose the spacetime metric g_{ab} as

$$g_{ab} = h_{ab} - U_aU_b, \tag{A2}$$

where h_{ab} is called the transverse metric. The metric h_{ab} is spatial in the sense that it is orthogonal to the timelike U^a

$$h_{ab}U^b = 0 = h_{ab}U^a \tag{A3}$$

which is simple to check from Equation (A2). It is also essentially a three dimensional metric on the hypersurfaces transverse to U^a, and this can be seen by taking the trace of Equation (A2) which leads to $h^a{}_a = 3$. The $(1,1)$ tensor $h^a{}_b$ is a projection operator onto the transverse hypersurfaces to U^a since $B^a{}_cB^c{}_b = B^a{}_b$, which can also be seen from Equation (A2).

In order to study the evolution of the congruence, we consider the tensor

$$B_{ab} = \nabla_b U_a, \tag{A4}$$

which is sometimes called the expansion tensor, and its $B^a{}_b$ version measures the amount of failure of the deviation vector between the geodesics in the congruence from being parallel transported. This tensor is also spatial since it is orthogonal to U^a

$$B_{ab}U^b = 0 = B_{ab}U^a. \tag{A5}$$

This is the result of the curves being geodesics, i.e., Equation (A1).

We algebraically decompose B_{ab} into its trace part, symmetric traceless part and antisymmetric part as

$$B_{ab} = \frac{1}{3}\theta h_{ab} + \sigma_{ab} + \omega_{ab}. \tag{A6}$$

Here

$$\theta = B^a{}_a \tag{A7}$$

is the trace of B_{ab} and is called the expansion scalar, and describes the fractional change of the area of the cross-section area of the congruence per unit time. The symmetric traceless part

$$\sigma_{ab} = B_{(ab)} - \frac{1}{3}\theta h_{ab} \tag{A8}$$

is called the shear tensor. It measures how the cross-section is deformed from a circle. The antisymmetric part

$$\omega_{ab} = B_{[ab]} \tag{A9}$$

is called the vorticity (or rotation) tensor, and encodes the overall rotation of the cross-section while the area remains unchanged. The factor $\frac{1}{3}$ is the result of the transverse hypersurfaces being three dimensional. Both σ_{ab} and ω_{ab} are spatial tensors, i.e., and their contraction with U^a vanishes.

These quantities and their rates of change along the geodesic in proper time incorporate important information about the structure of spacetime particularly, the geodesics incompleteness and singularities. The most important of these rates of change is the rate of change of the expansion scalar along the geodesics, $\frac{d\theta}{d\tau}$, where τ is the proper time along the geodesic. It can be computed to yield

$$U^a \nabla_a \theta := \frac{d\theta}{d\tau} = -\frac{1}{3}\theta^2 - \sigma_{ab}\sigma^{ab} + \omega_{ab}\omega^{ab} - R_{ab}U^a U^b. \tag{A10}$$

Here, $\sigma^2 = \sigma_{ab}\sigma^{ab}$ is called the shear parameter and $\omega^2 = \omega_{ab}\omega^{ab}$ is the vorticity parameter. In the presence of matter that obeys strong energy condition the last term $R_{ab}U^a U^b$ is always nonnegative, and it vanishes for the vacuum case.

The above equation is called the Raychaudhuri equation, and is a purely geometrical identity. Since σ_{ab} and ω_{ab} are spatial tensors, $\sigma^2 > 0$, $\omega^2 > 0$. So, in cases where the strong energy condition holds, the first second and the fourth terms on the right hand side of Equation (A10) (including the signs behind them) are all negative and contribute to the convergence of geodesics as we move along them. The only term with a positive sign is the third term ω^2, which contributes to divergence of geodesics. Hence, if it was not for the vorticity parameter, the rate of change of the expansion scalar would always have been negative, which leads to the geodesics increasingly converge as we move along them. In fact this is the case where U^a are hypersurface-orthogonal. In that case we have

$$\frac{d\theta}{d\tau} \leq -\frac{1}{3}\theta^2 \tag{A11}$$

which can be solved to yield

$$\frac{1}{\theta(\tau)} \geq \frac{1}{\theta(\tau_0)} + \frac{1}{3}\tau. \tag{A12}$$

Then if we have an initially-converging congruence, i.e., $\theta(\tau_0) < 0$, we arrive at a caustic point where $\theta \to -\infty$ in a finite proper time

$$\tau \leq -3\frac{1}{\theta(\tau_0)}. \tag{A13}$$

This caustic point could be the result of bad coordinates or a real physical singularity in spacetime. The Raychaudhuri equation is the backbone of the theorems of Hawking and Penrose about geodesic incompleteness and singularities in general spacetimes.

Appendix A.2. Null Congruence

For the null congruences with geodesics parametrized by λ, we consider the subspace normal to the null vector field k^a tangent to the geodesics. To do that, introduce a auxiliary null vector field l^a such that

$$k_a l^a = -1. \tag{A14}$$

Using these two null vectors, we can decompose the metric as

$$g_{ab} = h_{ab} - 2k_{(a}l_{b)}, \tag{A15}$$

where once again h_{ab} is the transverse metric on the hypersurface transverse to k^a and l^a. This hypersurface and its metric h_{ab} is two dimensional which can be confirmed by noticing $h^a{}_a = 2$. The tensor $h^a{}_b$ is again a projection operator onto these transverse hypersurfaces.

We can once again define

$$B_{ab} = \nabla_b k_a, \tag{A16}$$

but while this tensor is orthogonal to k^a, it is not orthogonal to l^a. It turns out the purely transverse part B_{ab},

$$\tilde{B}_{ab} = h^c{}_a h^d{}_b B_{cd} \tag{A17}$$

is the tensor that is orthogonal to both k^a and l^a. This tensor can explicitly written as

$$\tilde{B}_{ab} = B_{ab} + k_a l^c B_{cb} + k_b B_{ac} l^c + k_a k_b B_{cd} l^c l^d. \tag{A18}$$

Once again we can decompose $\tilde{B}_{ab}$ as

$$\tilde{B}_{ab} = \frac{1}{2}\tilde{\theta} h_{ab} + \tilde{\sigma}_{ab} + \tilde{\omega}_{ab}, \tag{A19}$$

where

$$\tilde{\theta} = \tilde{B}^a{}_a \tag{A20}$$

$$\tilde{\sigma}_{ab} = \tilde{B}_{(ab)} - \frac{1}{2}\theta h_{ab} \tag{A21}$$

$$\tilde{\omega}_{ab} = \tilde{B}_{[ab]} \tag{A22}$$

are the expansion scalar, and shear and vorticity tenors, respectively. The factor $\frac{1}{2}$ is the result of the transverse hypersurfaces being two dimensional. Again, both $\tilde{\sigma}_{ab}$ and $\tilde{\omega}_{ab}$ are spatial tensors.

The Raychaudhuri equation is now derived by considering the evolution of $\tilde{\theta}$ along the geodesics

$$k^a \nabla_a \tilde{\theta} := \frac{d\tilde{\theta}}{d\lambda} = -\frac{1}{2}\tilde{\theta}^2 - \tilde{\sigma}_{ab}\tilde{\sigma}^{ab} + \tilde{\omega}_{ab}\tilde{\omega}^{ab} - R_{ab}k^a k^b. \tag{A23}$$

Notice that $\tilde{\theta}$ is unique and independent of l^a since $\tilde{\theta} = \tilde{B}^a{}_a = B^a{}_a = \nabla_a k^a$, and so is the Raychaudhuri equation above. The interpretation of Equation (A23) is similar to the to the timelike case and leads to the existence of caustic points in many situations.

In what follows we will use both the expansion and the Raychaudhuri equation for both the null and timelike cases to study the effective behavior of the interior of the Schwarzschild black hole.

Note

[1] We use lower case Latin letter for abstract indices and Greek indices for components.

References

1. Thiemann, T. *Modern Canonical Quantum General Relativity*; Cambridge University Press: Cambridge, UK, 2007. [CrossRef]
2. Ashtekar, A.; Bojowald, M. Quantum geometry and the Schwarzschild singularity. *Class. Quant. Grav.* **2006**, *23*, 391–411. [CrossRef]
3. Bojowald, M. Spherically symmetric quantum geometry: States and basic operators. *Class. Quant. Grav.* **2004**, *21*, 3733–3753. [CrossRef]
4. Bojowald, M.; Swiderski, R. Spherically symmetric quantum geometry: Hamiltonian constraint. *Class. Quant. Grav.* **2006**, *23*, 2129–2154. [CrossRef]
5. Böhmer, C.G.; Vandersloot, K. Loop Quantum Dynamics of the Schwarzschild Interior. *Phys. Rev. D* **2007**, *76*, 104030. [CrossRef]
6. Corichi, A.; Singh, P. Loop quantization of the Schwarzschild interior revisited. *Class. Quant. Grav.* **2016**, *33*, 055006. [CrossRef]
7. Ashtekar, A.; Olmedo, J.; Singh, P. Quantum extension of the Kruskal spacetime. *Phys. Rev. D* **2018**, *98*, 126003. [CrossRef]
8. Ben Achour, J.; Lamy, F.; Liu, H.; Noui, K. Polymer Schwarzschild black hole: An effective metric. *Europhys. Lett.* **2018**, *123*, 20006. [CrossRef]
9. Bodendorfer, N.; Mele, F.M.; Münch, J. Effective Quantum Extended Spacetime of Polymer Schwarzschild Black Hole. *Class. Quant. Grav.* **2019**, *36*, 195015. [CrossRef]
10. Bodendorfer, N.; Mele, F.M.; Münch, J. (b,v)-Type Variables for Black to White Hole Transitions in Effective Loop Quantum Gravity. 2019. Available online: https://arxiv.org/abs/1911.12646 (accessed on 1 May 2022).
11. Bojowald, M.; Brahma, S.; Yeom, D.H. Effective line elements and black-hole models in canonical loop quantum gravity. *Phys. Rev. D* **2018**, *98*, 046015. [CrossRef]
12. Campiglia, M.; Gambini, R.; Pullin, J. Loop quantization of spherically symmetric midi-superspaces: The Interior problem. *AIP Conf. Proc.* **2008**, *977*, 52–63. [CrossRef]
13. Chiou, D.W. Phenomenological loop quantum geometry of the Schwarzschild black hole. *Phys. Rev. D* **2008**, *78*, 064040. [CrossRef]

14. Corichi, A.; Karami, A.; Rastgoo, S.; Vukašinac, T. Constraint Lie algebra and local physical Hamiltonian for a generic 2D dilatonic model. *Class. Quant. Grav.* **2016**, *33*, 035011. [CrossRef]
15. Cortez, J.; Cuervo, W.; Morales-Técotl, H.A.; Ruelas, J.C. Effective loop quantum geometry of Schwarzschild interior. *Phys. Rev. D* **2017**, *95*, 064041. [CrossRef]
16. Gambini, R.; Pullin, J. Black holes in loop quantum gravity: The Complete space-time. *Phys. Rev. Lett.* **2008**, *101*, 161301. [CrossRef]
17. Gambini, R.; Pullin, J.; Rastgoo, S. Quantum scalar field in quantum gravity: The vacuum in the spherically symmetric case. *Class. Quant. Grav.* **2009**, *26*, 215011. [CrossRef]
18. Gambini, R.; Pullin, J.; Rastgoo, S. Quantum scalar field in quantum gravity: The propagator and Lorentz invariance in the spherically symmetric case. *Gen. Rel. Grav.* **2011**, *43*, 3569–3592. [CrossRef]
19. Gambini, R.; Pullin, J. Loop quantization of the Schwarzschild black hole. *Phys. Rev. Lett.* **2013**, *110*, 211301. [CrossRef]
20. Gambini, R.; Olmedo, J.; Pullin, J. Spherically symmetric loop quantum gravity: Analysis of improved dynamics.*Class. Quant. Grav.* **2020**, *37*, 205012. [CrossRef]
21. Husain, V.; Winkler, O. Quantum resolution of black hole singularities. *Class. Quant. Grav.* **2005**, *22*, L127–L134. [CrossRef]
22. Husain, V.; Winkler, O. Quantum Hamiltonian for gravitational collapse. *Phys. Rev. D* **2006**, *73*, 124007. [CrossRef]
23. Kelly, J.G.; Santacruz, R.; Wilson-Ewing, E. Effective Loop Quantum Gravity Framework for Vacuum Spherically Symmetric Space-Times. 2020. Available online: https://arxiv.org/abs/2006.09302 (accessed on 1 May 2022).
24. Modesto, L. Loop quantum black hole. *Class. Quant. Grav.* **2006**, *23*, 5587–5602. [CrossRef]
25. Modesto, L.; Premont-Schwarz, I. Self-dual Black Holes in LQG: Theory and Phenomenology. *Phys. Rev. D* **2009**, *80*, 064041. [CrossRef]
26. Olmedo, J.; Saini, S.; Singh, P. From black holes to white holes: A quantum gravitational, symmetric bounce. *Class. Quant. Grav.* **2017**, *34*, 225011. [CrossRef]
27. Thiemann, T.; Kastrup, H. Canonical quantization of spherically symmetric gravity in Ashtekar's selfdual representation. *Nucl. Phys. B* **1993**, *399*, 211–258. [CrossRef]
28. Zhang, C.; Ma, Y.; Song, S.; Zhang, X. Loop quantum Schwarzschild interior and black hole remnant. *Phys. Rev. D* **2020**, *102*, 041502. [CrossRef]
29. Ziprick, J.; Gegenberg, J.; Kunstatter, G. Polymer Quantization of a Self-Gravitating Thin Shell.*Phys. Rev. D* **2016**, *94*, 104076. [CrossRef]
30. Campiglia, M.; Gambini, R.; Pullin, J. Loop quantization of spherically symmetric midi-superspaces. *Class. Quant. Grav.* **2007**, *24*, 3649–3672. [CrossRef]
31. Gambini, R.; Pullin, J.; Rastgoo, S. New variables for 1+1 dimensional gravity. *Class. Quant. Grav.* **2010**, *27*, 025002. [CrossRef]
32. Rastgoo, S. A local true Hamiltonian for the CGHS Model in New Variables. 2013. Available online: https://arxiv.org/abs/1304.7836 (accessed on 1 May 2022).
33. Corichi, A.; Olmedo, J.; Rastgoo, S. Callan-Giddings-Harvey-Strominger vacuum in loop quantum gravity and singularity resolution. *Phys. Rev. D* **2016**, *94*, 084050. [CrossRef]
34. Morales-Técotl, H.A.; Rastgoo, S.; Ruelas, J.C. Effective dynamics of the Schwarzschild black hole interior with inverse triad corrections. *Annals. Phys.* **2021**, *426*, 168401. [CrossRef]
35. Ben Achour, J.; Brahma, S.; Uzan, J.P. Bouncing compact objects. Part I. Quantum extension of the Oppenheimer-Snyder collapse. *J. Cosmol. Astropart. Phys.* **2020**, *3*, 41. [CrossRef]
36. Blanchette, K.; Das, S.; Hergott, S.; Rastgoo, S. Black Hole Singularity Resolution via the Modified Raychaudhuri Equation in Loop Quantum Gravity. *Phys. Rev. D* **2021**, *103*, 084038. [CrossRef]
37. Husain, V.; Kelly, J.G.; Santacruz, R.; Wilson-Ewing, E. On the Fate of Quantum Black Holes. 2022. Available online: https://arxiv.org/abs/2203.04238 (accessed on 1 May 2022).
38. Addazi, A.; Alvarez-Muniz, J.; Batista, R.A.; Amelino-Camelia, G.; Antonelli, V.; Arzano, M.; Asorey, M.; Atteia, J.L.; Bahamonde, S.; Bajardi, F. Quantum gravity phenomenology at the dawn of the multi-messenger era—A review. *Prog. Part. Nucl. Phys.* **2021**, *125*, 103948. [CrossRef]
39. Assanioussi, M.; Mickel, L. Loop effective model for Schwarzschild black hole interior: A modified $\bar{\mu}$ dynamics. *Phys. Rev. D* **2021**, *103*, 124008. [CrossRef]
40. Husain, V.; Kelly, J.G.; Santacruz, R.; Wilson-Ewing, E. Quantum Gravity of Dust Collapse: Shock Waves from Black Holes. *Phys. Rev. Lett.* **2022**, *128*, 121301. [CrossRef]
41. Assanioussi, M.; Dapor, A.; Liegener, K. Perspectives on the dynamics in a loop quantum gravity effective description of black hole interiors. *Phys. Rev. D* **2020**, *101*, 026002. [CrossRef]
42. Ashtekar, A.; Fairhurst, S.; Willis, J.L. Quantum gravity, shadow states, and quantum mechanics. *Class. Quant. Grav.* **2003**, *20*, 1031–1062. [CrossRef]
43. Corichi, A.; Vukasinac, T.; Zapata, J.A. Polymer Quantum Mechanics and its Continuum Limit. *Phys. Rev. D* **2007**, *76*, 044016. [CrossRef]
44. Morales-Técotl, H.A.; Rastgoo, S.; Ruelas, J.C. Path integral polymer propagator of relativistic and nonrelativistic particles. *Phys. Rev. D* **2017**, *95*, 065026. [CrossRef]

45. Morales-Técotl, H.A.; Orozco-Borunda, D.H.; Rastgoo, S. Polymer quantization and the saddle point approximation of partition functions. *Phys. Rev. D* **2015**, *92*, 104029. [CrossRef]
46. Flores-González, E.; Morales-Técotl, H.A.; Reyes, J.D. Propagators in Polymer Quantum Mechanics. *Ann. Phys.* **2013**, *336*, 394–412. [CrossRef]
47. Ashtekar, A.; Pawlowski, T.; Singh, P. Quantum nature of the big bang. *Phys. Rev. Lett.* **2006**, *96*, 141301. [CrossRef]
48. Ashtekar, A.; Pawlowski, T.; Singh, P. Quantum Nature of the Big Bang: An Analytical and Numerical Investigation. I. *Phys. Rev. D* **2006**, *73*, 124038. [CrossRef]
49. Joe, A.; Singh, P. Kantowski-Sachs spacetime in loop quantum cosmology: Bounds on expansion and shear scalars and the viability of quantization prescriptions. *Class. Quant. Grav.* **2015**, *32*, 015009. [CrossRef]
50. Saini, S.; Singh, P. Geodesic completeness and the lack of strong singularities in effective loop quantum Kantowski–Sachs spacetime. *Class. Quant. Grav.* **2016**, *33*, 245019. [CrossRef]
51. Alesci, E.; Bahrami, S.; Pranzetti, D. Quantum gravity predictions for black hole interior geometry. *Phys. Lett. B* **2019**, *797*, 134908. [CrossRef]
52. Alesci, E.; Bahrami, S.; Pranzetti, D. Asymptotically de Sitter universe inside a Schwarzschild black hole. *Phys. Rev. D* **2020**, *102*, 066010. [CrossRef]
53. Das, S.; Vagenas, E.C. Universality of Quantum Gravity Corrections. *Phys. Rev. Lett.* **2008**, *101*, 221301. [CrossRef] [PubMed]
54. Ali, A.F.; Das, S.; Vagenas, E.C. A proposal for testing Quantum Gravity in the lab. *Phys. Rev. D* **2011**, *84*, 044013. [CrossRef]
55. Blanchette, K.; Das, S.; Rastgoo, S. Effective GUP-modified Raychaudhuri equation and black hole singularity: Four models. *J. High Energy Phys.* **2021**, *09*, 062. [CrossRef]
56. Bosso, P.; Obregón, O.; Rastgoo, S.; Yupanqui, W. Deformed Algebra and the Effective Dynamics of the Interior of Black. 2020. Available online: https://arxiv.org/abs/2012.04795 (accessed on 1 May 2022).
57. Villalpando, C.; Modak, S.K. Indirect Probe of Quantum Gravity using Molecular Wave-packets. *Class. Quant. Grav.* **2019**, *36*, 215016. [CrossRef]
58. Das, S.; Fridman, M.; Lambiase, G.; Vagenas, E.C. Baryon asymmetry from the generalized uncertainty principle. *Phys. Lett. B* **2022**, *824*, 136841. [CrossRef]
59. Mignemi, S. Extended uncertainty principle and the geometry of (anti)-de Sitter space. *Mod. Phys. Lett. A* **2010**, *25*, 1697–1703. [CrossRef]
60. Costa Filho, R.N.; Braga, J.a.P.M.; Lira, J.H.S.; Andrade, J.S. Extended uncertainty from first principles. *Phys. Lett. B* **2016**, *755*, 367–370. [CrossRef]
61. Schürmann, T. On the uncertainty principle in Rindler and Friedmann spacetimes. *Eur. Phys. J. C* **2020**, *80*, 141. [CrossRef]
62. Dabrowski, M.P.; Wagner, F. Extended Uncertainty Principle for Rindler and cosmological horizons. *Eur. Phys. J. C* **2019**, *79*, 716. [CrossRef]
63. Hamil, B.; Merad, M.; Birkandan, T. Applications of the extended uncertainty principle in AdS and dS spaces. *Eur. Phys. J. Plus* **2019**, *134*, 278. [CrossRef]
64. Giné, J.; Luciano, G.G. Modified inertia from extended uncertainty principle(s) and its relation to MoND. *Eur. Phys. J. C* **2020**, *80*, 1039. [CrossRef]
65. Wagner, F. Relativistic extended uncertainty principle from spacetime curvature. *Phys. Rev. D* **2022**, *105*, 025005. [CrossRef]
66. Blanchette, K.; Das, S.; Hergott, S.; Rastgoo, S. Effective black hole interior and the Raychadhuri equation. In Proceedings of the 16th Marcel Grossmann Meeting on Recent Developments in Theoretical and Experimental General Relativity, Astrophysics and Relativistic Field Theories, Online, Italy, 5–9 July 2021. Available online: https://arxiv.org/abs/2110.05397 (accessed on 1 May 2022).
67. Collins, C. Global structure of the Kantowski-Sachs cosmological models. *J. Math. Phys.* **1977**, *18*, 2116. [CrossRef]
68. Chiou, D.W. Phenomenological dynamics of loop quantum cosmology in Kantowski-Sachs spacetime. *Phys. Rev. D* **2008**, *78*, 044019. [CrossRef]
69. Morales-Técotl, H.A.; Orozco-Borunda, D.H.; Rastgoo, S. Polymerization, the Problem of Access to the Saddle Point Approximation, and Thermodynamics. In Proceedings of the 14th Marcel Grossmann Meeting on Recent Developments in Theoretical and Experimental General Relativity, Astrophysics, and Relativistic Field Theories, Rome, Italy, 12–18 July 2017; Volume 4, pp. 4054–4059.
70. Modesto, L. Semiclassical loop quantum black hole. *Int. J. Theor. Phys.* **2010**, *49*, 1649–1683. [CrossRef]
71. Ashtekar, A.; Pawlowski, T.; Singh, P. Quantum Nature of the Big Bang: Improved dynamics. *Phys. Rev. D* **2006**, *74*, 084003. [CrossRef]
72. Ashtekar, A.; Wilson-Ewing, E. Loop quantum cosmology of Bianchi I models. *Phys. Rev. D* **2009**, *79*, 083535. [CrossRef]